This article is a non-peer-reviewed preprint.

Assessing the riverine flood forecast skill of GloFAS and Google Flood Hub with impact data and discharge observations to support early actions in Mali

Els Kuipers[1,2], Valentijn Oldenburg[1], Phuoc Phung[1], Edwin H. Sutanudjaja[2], Andrea Ficchì[3], Peter Salamon[4], Marc van den Homberg[1,5]
[1]The Netherlands Red Cross‘ data and digital team 510, Netherlands
[2]Department of Physical Geography, Faculty of Geosciences, Utrecht University, Netherlands
[3]Department of Electronics, Information, and Bioengineering, Politecnico di Milano, Italy
[4]European Commission, Joint Research Centre, Ispra, Italy
[5]Faculty of Geo-Information Science and Earth Observation/ITC, University of Twente, Netherlands

0. Abstract

Riverine floods are among the most destructive and frequent natural hazards in Mali. To reduce their impacts, the Mali Red Cross implemented an Early Action Protocol (EAP) to enable anticipatory actions through pre-defined triggers and forecast information. Currently, the protocol relies on upstream water levels from the National Directorate of Hydraulics (DNH) to predict downstream flooding. However, this model does not consider meteorological forcing, limiting lead times to a maximum of four days. Recent advancements in global flood forecasting systems present opportunities to enhance Mali's EAP by leveraging increasingly skilful medium-range weather forecasts as inputs of both physics-based models, as in the Global Flood Awareness System (GloFAS), and AI-based models, as in Google Flood Hub (GFH). We compare GloFAS v4.0 and v3.0, GFH, and Mali’s current trigger model using discharge observations and district-level impact data derived from multiple sources and text-mined news-articles. Model performance was assessed for a range of lead times and discharge thresholds. GloFAS and GFH demonstrate sufficient skill for early action beyond 4-day lead time in frequently flooded regions and have a larger spatial coverage compared to the current trigger model, suggesting early action plans could operate with 7-day lead time and span a larger area. Overall, this study highlights the potential and challenges of flood forecasting for anticipatory action in flood-prone, data-scarce regions. In particular, we (i) assess the usability of two different ground truths (observed discharge and impact data) for forecast validation; (ii) assess the possibility of extending Mali’s current trigger model in lead time and spatial coverage; and (iii) evaluate user-oriented forecast skill across models and contexts.

Keywords: riverine floods, anticipatory action, trigger model, impact-based forecasting, forecast verification, GloFAS, Google Flood Hub

1. Introduction

Riverine floods rank among the most frequent and destructive natural hazards in Mali (Croix-Rouge Malienne et al., 2023). With climate change, floods are expected to increase in intensity and frequency, and so is their impact on livelihoods (Hirabayashi et al., 2013). Early warning systems (EWS) can provide critical early insights for local communities, governments, and humanitarian aid organizations, enabling anticipatory actions with the potential to protect lives and livelihoods (Alfieri, 2013). Because of its effectiveness (Kousky et al., 2019; Rai et al., 2020; WFP, 2025), humanitarian aid has in recent years been shifting from reactive to anticipatory, where Early Action Protocols (EAPs) rely on forecasting systems (Mitheu et al., 2023).

Mali is vulnerable to riverine flooding due to its semi-arid climate and the heavy rains brought by the West African Monsoon (De Filippis et al., 2022). Flood risk is particularly severe in populated regions surrounding the Niger and Senegal rivers, including the urban areas of Mopti, Ségou, Bamako, Koulikoro, Timbuktu and Gao (Croix-Rouge Malienne et al., 2023). Mali's climatic conditions, as well as socio-economic pressures, like conflict, population growth, irrigation, and dam construction, exacerbate its exposure and vulnerability to floods (De Filippis et al., 2022; Yue et al., 2022; Skidmore et al., 2016; Andersen et al., 2001). The frequency and impact of floods increased significantly, with rises in fatalities, injuries, and damage to infrastructure and livelihoods (DGPC, 2018). In 2018 alone, floods affected 137.000 people nationwide (DGPC, 2018). Despite this recurrence, humanitarian action in Mali remains predominantly reactive, mostly focusing on post-disaster response.

Recent advancements in global flood forecasting systems have pushed the limits of skilful lead times, spatial resolution and accuracy (Harrigan et al., 2023; Nearing et al., 2024; Matthews et al., 2025) increasing their potential to support EAPs. Moreover, impact-based forecasting represents a key advancement in flood forecasting, focusing not on what the weather will be but on what it will do (Merz et al., 2020). This requires linking of hydrological (river discharge) predictions to binary definitions of impact (Coughlan de Perez et al., 2016; Harrison et al., 2022; Mitheu et al., 2023). Hydrological forecasts predict hazard parameters like river discharge levels (e.g., Alfieri, 2013) and flood inundation extent or flood depth (e.g., Dottori et al., 2016; Riedel et al., 2024), which are then coupled with vulnerability and exposure datasets to assess potential damages (Harrison et al., 2022).

Humanitarian anticipatory action operationalises these forecast advancements by ensuring that funds are secured ahead of an extreme event, to trigger early actions when predefined impact levels are forecasted (Coughlan de Perez et al., 2015). Triggers are defined by thresholds of a hazard or impact variable, selected and reported in EAPs based on local historical risk assessments and stakeholders' expert-based preferences, marking the expected onset of humanitarian impact. To prevent frequent actions in vain and straining of the system, forecasts should be sufficiently skilful and associated with unlikely false alarms as well as a high probability of detecting an actual impact well in advance. This ensures credibility, communal trust, and financial sustainability. Therefore, trigger thresholds of a return period greater than five years are often employed (Coughlan de Perez et al., 2015; Pagano et al., 2024).

Gaps and challenges persist in developing and calibrating flood forecast models in data-scarce regions. In Mali, scarce observational hazard and impact data (Salinas et al., 2013; Kan et al., 2017; Yue et al., 2022; Mitheu et al., 2023), along limited operational technologies for localized river discharge modelling (Akpoti et al., 2024; Fofana et al., 2023), limit the deployment, validation and skill assessments of weather and flood forecasts. Decision-making is further complicated by Mali's highly variable climate (Zeng, 2003; Traoré et al., 2007). State-of-the-art global forecasting systems can form an alternative, but they are, in most parts of Sub-Saharan Africa, poorly calibrated and have a mostly unknown predictive accuracy, both because of said data-scarcity (e.g., Revilla-Romero et al., 2015; Harrigan et al., 2023). Only a few per cent of the world's watersheds are gauged, and stream gauges are not distributed evenly across the globe, with low GDP countries relying in particular on ungauged watersheds and therefore poorly calibrated and validated forecasts (Nearing et al., 2024). This is particularly problematic because it is especially in these countries that communities vulnerable to the impacts of flooding live.

In Mali, these limitations hamper the possible scale-up of the current trigger model for flood-related anticipatory action, which has limited spatial coverage and lead time. The propagation trigger model (PTM) used by the latest flood EAP in Mali, as approved in March 2025, assumes propagation of water from upstream to downstream river gauges, triggering when upstream water levels surpass the 5-year return period threshold, while assuming a lag time for the discharge to propagate to the downstream station (Croix-Rouge Malienne et al., 2023). These water levels are monitored by the National Hydraulics Directorate (Direction Nationale de l'Hydraulique, DNH-Mali) along the Niger river (Croix-Rouge Malienne et al., 2023). Since the PTM does not integrate meteorological and hydrological forecasts, it fails to account for large spatial and temporal variations, covers only few river gauges in Mali, and has a maximum lead time of four days.

Integrating weather forecasts with hydrological modelling could enhance the predictive accuracy, the spatial coverage and lead time of the trigger model. To assess this hypothesis, our study analyses two state-of-the-art global flood forecasting systems that do integrate extended-range lead time meteorological forecasts, i.e. a physics-based system (GloFAS) and an AI-based one (Google Flood Hub).

The Global Flood Awareness System (GloFAS) of the Copernicus Emergency Management Service (CEMS) was developed to provide global, real-time flood forecasts in large transboundary river basins by combining ensemble weather predictions with hydrological modelling (Alfieri et al., 2013; Matthews et al., 2025). GloFAS runs to a large extent in a parameter-regionalization mode, meaning that model parameters are fixed based on global datasets such as land cover, soils, topography rather than always calibrated against dense local discharge records (Alfieri et al., 2013). Whenever possible, GloFAS is regularly updated and improved, also benefiting from an increasing number of observations shared by national hydrological agencies worldwide. The latest operational GloFAS version (v4.0) has brought a significantly enhanced hydrological model calibration, through new observation points including also several stations in Mali, and an increased spatial resolution of approximately 5 by 5 km (0.05°). Thanks to this, the model is expected to have an increasing potential for triggering future anticipatory actions, while minimizing the risk of false alarms or of overlooking major flood events. By including GloFAS v3.0 in the analysis, we test whether the improvements introduced in GloFAS v4.0 translate into better performance also in an impact-based forecasting setting for a data-scarce region.

AI-based models have potential in terms of improving forecast skill in areas where there is no locally-calibrated hydrological model, given their ability to generalise across ungauged, data-scarce regions (Kratzert et al., 2019). Google Flood Hub (GFH) by Google Research (Nearing et al., 2024; Cohen, D., 2024) provides real-time, AI-based flood forecasts with a 7-day lead time in over 150 countries. In contrast to the global physics-based gridded model used by GloFAS, GFH delivers point-based timeseries forecasts distributed over more than one million points along rivers worldwide (Cohen, D. 2024).

Leveraging on these recent advancements of the GloFAS and GFH systems, this study evaluates and compares the riverine flood forecast skill of GloFAS v4.0, GFH and the current PTM for Mali's flood-prone areas, in the Niger and Senegal river basins. Evaluations of flood forecasting models usually focus on measuring performance against gauged river discharge observations over a multi-year period and independently from whether a flood event leads to impact, using generalist performance metrics, such as Nash-Sutcliffe or Kling-Gupta Efficiency (e.g., Prudhomme et al. 2024). However, the use of a flood forecasting model for anticipatory action requires a user-centred evaluation (e.g., Loveday et al., 2024; Pagano et al., 2024; Hossain et al. 2024), focusing on how the flood forecasting model performs in terms of detecting events above a certain (impact-based) threshold value. In previous work in Mali (Van den Homberg et al., 2022a), such an analysis was conducted for GloFAS v3.0 with the preliminary conclusion that setting trigger levels for longer lead times (to complement the existing four-day PTM-based trigger) can be done only for those locations where enough historical observed data is available; in addition, using impact data to set triggers was found to be hampered by limitations of the impact dataset, such as no precise event dates and locations. Mitheu et al. (2023) investigated the potential of impact data to evaluate GloFAS riverine flood forecast skill, also highlighting the need of additional validation with ground-truth hydrological data.

This study contributes to improving flood early warning and anticipatory action in data-scarce contexts, such as Mali. It examines how and whether integrating global physics- and AI-based forecasting systems can strengthen existing trigger models and enable more reliable, earlier humanitarian responses. To verify the forecasts, we assess the usability of two ground truths: (a) station-level river discharge observations and (b) district-level impact data (including text-mined reports). In addition, we test whether GloFAS v3.0/v4.0 and GFH can improve on the PTM by (a) expanding spatial coverage and (b) extending actionable lead time from 4 to 7 days, for different flood severity levels. As a final contribution, we evaluate the user-oriented forecast skill across models and context. Models are compared across lead times, thresholds, data availability and we give insights and recommendations for deployment.

2. *Study area, flood forecasting models and data*

This section describes the PTM, GloFAS, and GFH models, and the data used in their development and analysis.

2.1. Study area: the Senegal and Niger river basin

Mali’s two major river systems, the Niger and Sénégal basins, are central to socio-economic development, supporting agriculture, fisheries, and diverse livelihoods, while exposing riverbank communities to frequent flooding. Both basins experience seasonal floods driven by the West African Monsoon, with observations and projections indicating increasing flood risk (Wilcox et al., 2018; Aich et al., 2016a, 2016b; Ndiaye et al., 2023).

The Niger River Basin, West Africa's largest (2.2 million km^2) and spanning ten countries, ranges from extremely wet headwaters to dry northern regions (Liersch et al., 2013). Flood peaks occur between July and January. In Mali, the Inner Niger Delta—a 350,000 km^2 floodplain—attenuates peak flows and supports fisheries, grazing, and flood-recession agriculture (Zare et al., 2017). Its complex flood propagation, long travel times, and sensitivity to upstream discharge, reservoirs, and rainfall variability make flood modeling and forecasting particularly challenging (Rebelo et al., 2013).

The Sénégal River Basin, West Africa's second largest (375,000 km^2), is shared by Guinea, Mali, Mauritania, and Senegal, and also exhibits high climate variability and monsoon dependence (Andersen et al., 2001). Floods peak between July and October. In Mali, the Manantali Dam on the Bafing River affects downstream hydrology but has limited impact on high-flow regulation (Sakho et al., 2017). Contrasting climates, spatial rainfall variability, and human regulation make hydrological modeling and reliable forecasts dependent on scarce local data (Sakho et al., 2017; Andersen et al., 2001)

2.2. Propagation Trigger Model (PTM)

From past streamflow observations as provided by DNH, a reforecast can be calculated based on the PTM in the current EAP. This trigger model is based on streamflow propagation times from upstream to downstream river gauges: downstream river gauges are related to upstream ones, and the lead time is the propagation time. In the model, flood triggers are activated when upstream water levels surpass the 5-year return period threshold, while assuming a lag time for the discharge to propagate to the downstream river gauge (Croix-Rouge Malienne et al., 2023). Figure 1 and 2 both show the stations' locations. Though the EAP is based on water levels instead of discharge measures, we used discharge as it was the best covering dataset. Among these stations, only 5 stations have a defined lag time that can be used for assessing the accuracy.

2.3. Global Flood Awareness System (GloFAS)

We evaluate the forecast skill of GloFAS v4.0, part of the Copernicus Emergency Management Service (CEMS), developed by the EU JRC and ECMWF (Matthews et al., 2025; Prudhomme et al., 2024), using reforecast data from 1999–2023 available via the Early Warning Data Store (EWDS). The dataset provides gridded river discharge at 0.05° resolution globally. Meteorological forcings come from ERA5 reanalysis for initial conditions and historical runs (GloFAS-ERA5), while reforecasts use ECMWF IFS ensemble forecasts. These forcings feed the open-source LISFLOOD hydrological model, which also takes into account static maps of hydrologically-relevant variables (e.g., land use, soil hydraulic properties, channel geometry, leaf area index, etc.) to produce the river discharge outputs, such as the reforecasts. In the latest GloFAS version, the LISFLOOD model is calibrated using data from 1995 reporting points with a minimum of 4-years-long timeseries of streamflow observations; a regionalisation approach is applied to transfer the parameters from gauged to ungauged catchments, to improve model capabilities in data-scarce regions.

Operationally, daily forecasts are publicly available (https://global-flood.emergency.copernicus.eu/), with lead times up to 15 days and consisting of 51 ensemble members representing forecast uncertainty. The reforecasts consist of 10 ensemble members and are run twice weekly using the latest operational version of the system. GloFAS offers reanalysis and reforecast datasets (e.g. Matthews et al., 2025), over 1979–2024 and 1999–2023, respectively. In this analysis, we use reforecasts up to 7 days lead time, consistently with the longest lead time available from the other product (see next section on Google Flood Hub reforecasts). In line with existing EAPs using GloFAS forecasts (Mitheu et al., 2023), a trigger level of 60% certainty is considered meaning the considered flood threshold is exceeded by 6 out of the 10 ensemble members for the historical analysis. Figure~1 displays an example of the raw gridded data together with DNH river gauges.

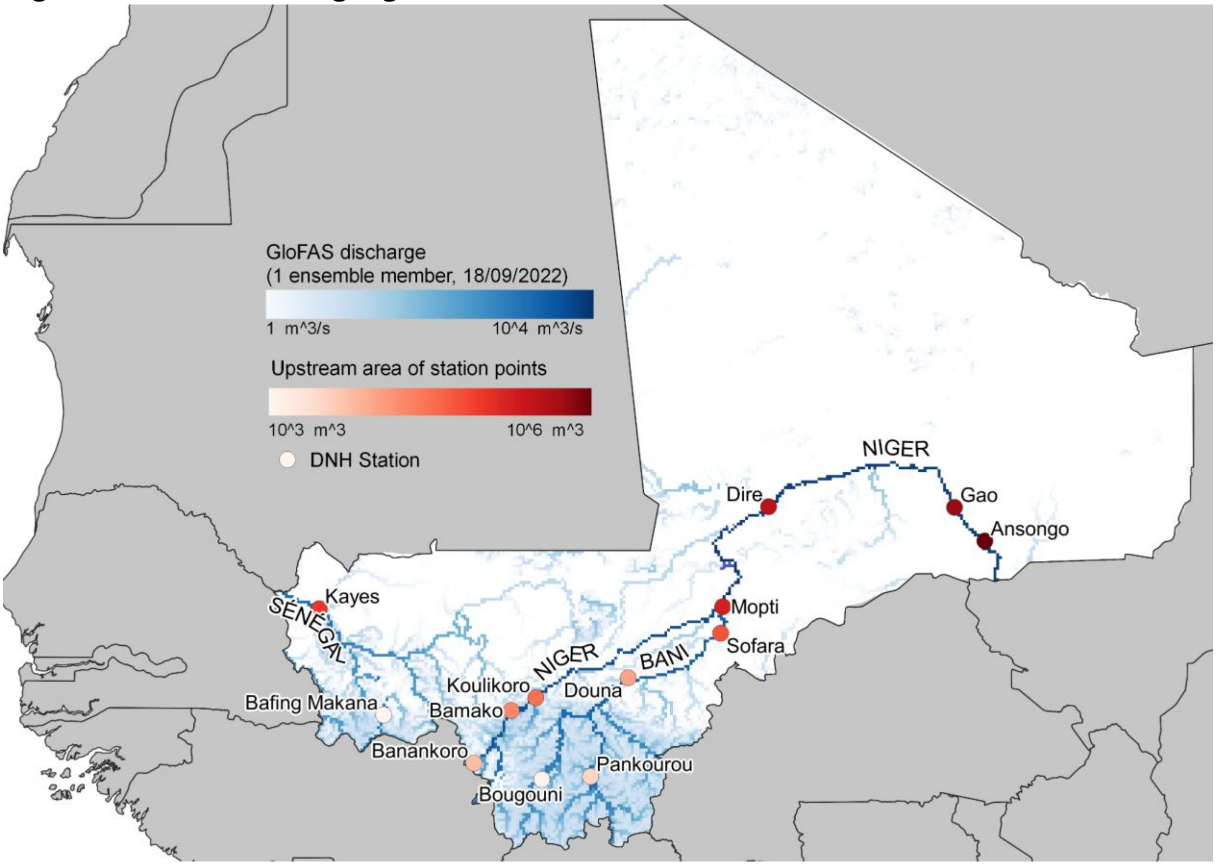

Figure 1: Map of Mali highlighting the 13 river gauges by DNH used in the study. Station colour associates a station to its upstream area (DNH, 2019). Larger upstream areas are associated with stations located more downstream in the river system (having collected more water from upstream contributing areas). The river network in the background is colored based on a GloFAS discharge forecast for one ensemble member with 7-day lead time for 18/09/2022. Natural Earth basemap. Stations Banankoro, Bamako, Koulikoro, Tamani and Kirango, are the stations included in the PTM with an established lag time.

2.4. Google Flood Hub (GFH)

Google Flood Hub (GFH) is an AI-driven flood forecasting platform that provides continuous, real-time global flood forecasts (Nearing et al., 2024). Its deep learning model combines various types of inputs using embedding networks (Cohen, D., 2024).

More specifically, it processes: (1) meteorological timeseries from multiple sources, including GraphCast, an AI-based medium-range global weather forecasting model (Lam, R., 2023), and the ECMWF ERA5-Land reanalysis dataset (Muñoz Sabater, J., 2019); and (2) hydrological and climatic catchment attributes from the HydroSHEDS dataset (Lehner and Grill, 2013). In addition, daily streamflow values from both the Global Runoff Data Center (GRDC) and the *\emph{Caravan}* dataset (Kratzert, F., 2023)—an open-source globally-standardised large-sample hydrology dataset—serve as training targets (i.e., calibration data). With these embedded inputs, it autoregressively generates discharge distributions over a 7-day lead time, from which it samples point predictions daily. The forecasts are issued daily and publicly available (https://g.co/floodhub).

Forecasts cover ~1 million virtual gauge points in HydroATLAS, divided into "verified" (historical streamflow available or inundation events verification from remote sensing images), and "unverified'' (ungauged and datascarce catchments) points (Linke et al, 2019). GFH's most recent version (Cohen, D., 2024) is trained with data from 15.980 virtual gauges, meaning most of the points' quality is un- or sparsely verified. Figure~2 shows the distribution of verified and unverified virtual gauges over Mali. We see non-excluded virtual gauges—either verified or unverified—line up with the Niger, Senegal, and Bani rivers. 16 verified virtual gauges are present in Mali, against 693 included unverified ones. Ideally, all gauges and locations would be verified; however, since verified virtual gauges are underrepresented, we use all virtual gauges indiscriminately.

Historical performance is assessed using the Google Runoff Reanalysis & Reforecast dataset (GRRR, 1980–2023 reanalysis; 2016–2022 reforecasts). Reanalyses use historical atmospheric data at 0-day lead time, while reforecasts simulate past forecasts, providing eight points per issue over the 7-day lead time.

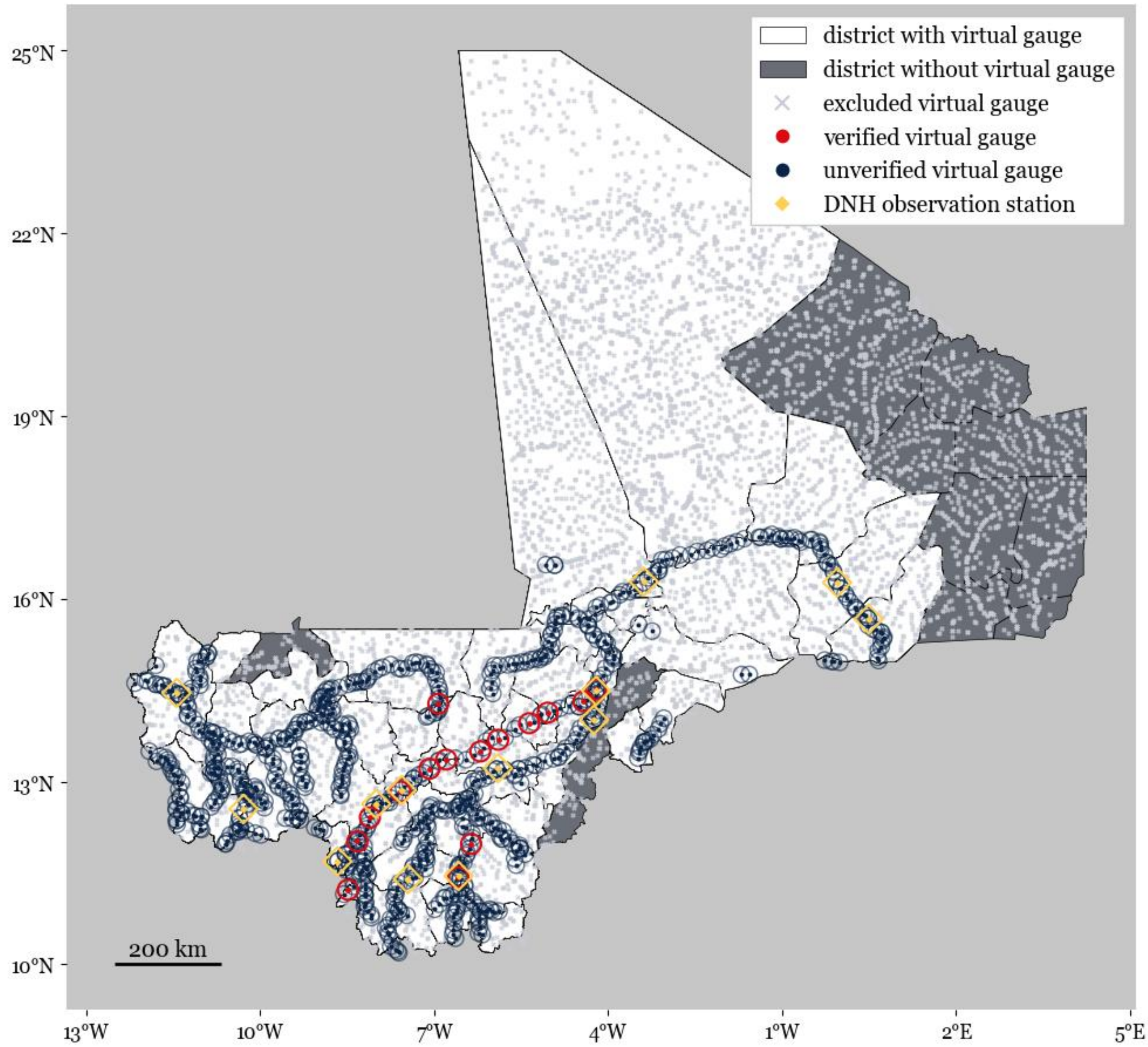

Figure 2: Distribution of Google Runoff Reanalysis Reforecast (GRRR) virtual gauges over Mali, classified as either verified, unverified, and excluded (points with 5-year return period threshold below \SI{100}{\cubic\metre\per\second}). Following the definition of excluded gauges, the Mali and Senegal river can be distinguished by gauges with higher extreme discharges. Administrative boundaries from Natural Earth (scale 1:110m, naturalearthdata.com).

2.5. Ground truth data: river discharge observations and impact data

The models are compared using a reference for impactful flood events coming from two sources: impact data, i.e. data recorded for occurred impactful flood events, and observation data, i.e. river discharges as observed at various river gauges through Mali.

Impact data can be defined as detailed information on the impact of past floods: when and where they happened, how many people died or got affected, which buildings and infrastructures got damaged or destroyed. The impact data is a compilation of data with different collection methods, temporal resolutions (e.g. monthly or quarterly), spatial resolutions (e.g. region-level vs. district-level), levels of detail, and flood (severity) definitions. The data are sourced from global impact repositories (EM-DAT, Desinventar and CatNat), global humanitarian data repositories (UN OCHA's Humanitarian Data

Exchange) and directly from national actors (such as the Direction Générale de la Protection Civile (DGPC)). The impact data was complemented with data from online news media articles between 2009 and 2017 using text mining (Van den Homberg et al., 2022b).

Observed daily discharge data from the network of the National mandated hydrological agency of Mali (Direction Nationale de l'Hydraulique du Mali, DNH MALI) is supplied for 14 river gauges, for which the locations are shown in Figure~1 and 2. Figure~3 shows a sample for Bamako, Mali's capital, including forecasts by GloFAS and GFH sampled from nearby points to get a sense of the data.

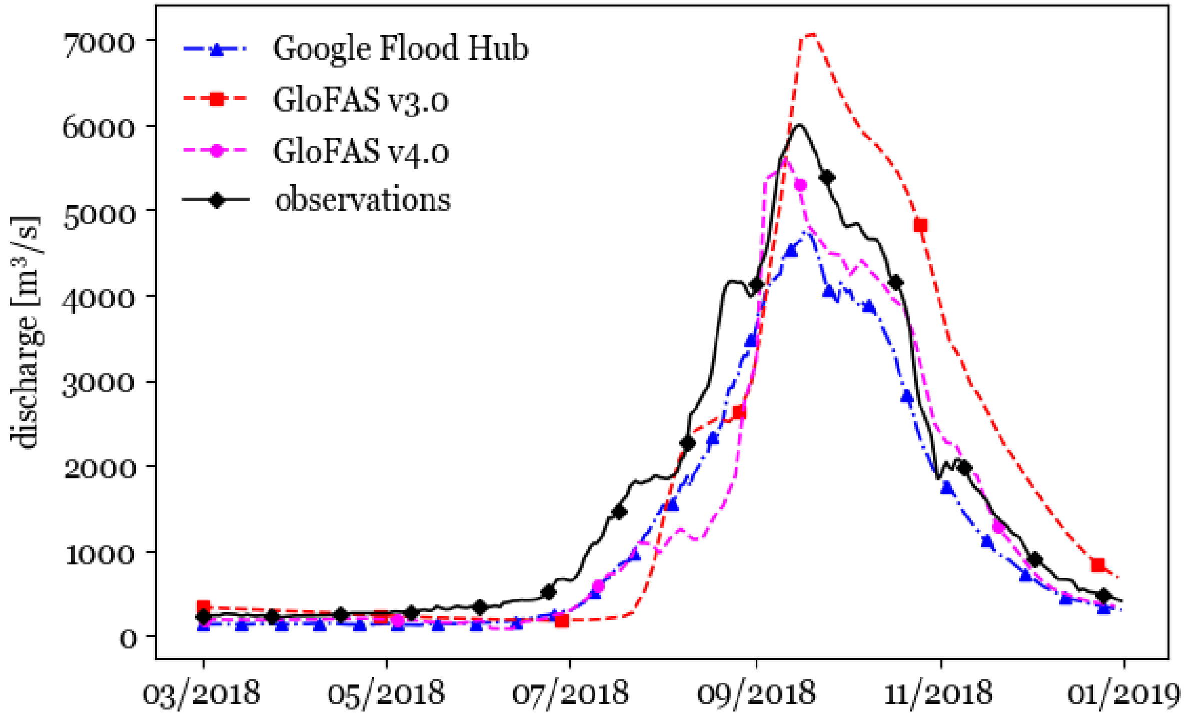

Figure 3: Timeseries plot showing a sample of Google Flood Hub-, GloFAS v3.0-, and GloFAS v4.0-forecasts with 4-day lead time and discharge observations taken near Bamako, Mali's capital, for 2018.

3. Methods to assess forecast skill

This section will provide a brief overview of the Methods, with details outlined in Appendix~B. To make the different types of data comparable, all data was transformed into a uniform "flood event" format, defined by location and duration. Forecasts and observation discharges were considered at a station-level, whose hydrographs were transformed into a set of events using threshold exceedances. Impact events were aggregated to the district-level. A flowchart of the full pipeline is shown in Figure~4.

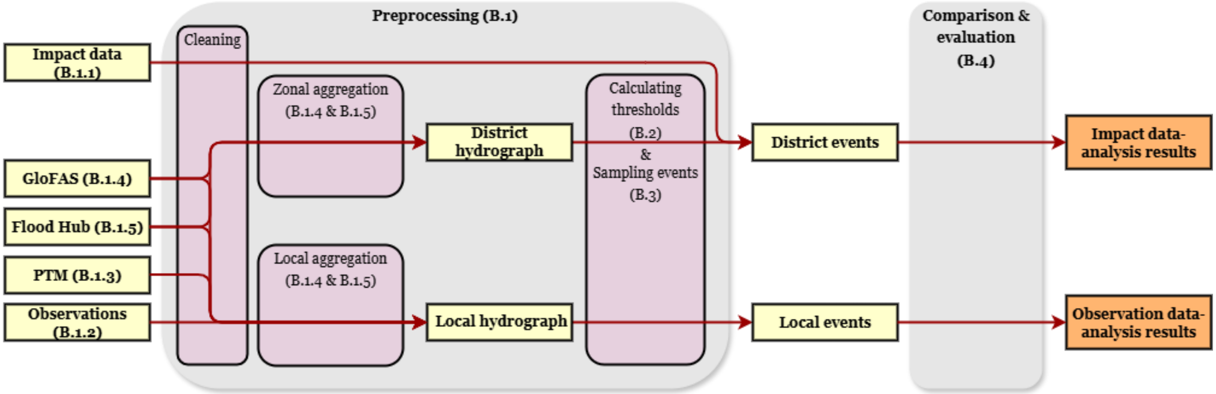

Figure 4: Flowchart showing the data pipeline with Section numbers appended. Raw data enters preprocessing on the left and leaves preprocessing as \emph{events}: impact data unites with zonally aggregated model forecasts to form district-level events for the impact data-analysis and observation data unites with locally aggregated model forecasts to form local station-level events for the observation data-analysis. Following their creation, the events are compared (ground truth versus forecast) over time and space to get to results.

Table 1: Considered timeframes and thresholds for the analyses of the impact and observation data. "RP'' denotes return period. The observation data-analysis is limited in timeframe and thresholds due to limited data availability; more ` ` rare" thresholds cease to be applicable.

	Impact data-analysis	*Observation data-analysis*
Analysis timeframe	01/01/16–31/12/2022	01/01/2016–31/12/2022
Return period thresholds Q_{th}	1.5-, 2-, 5-, 10-yr RP (computed from Gumbel fit on annual maxima),	1.5-, 2-, 5-yr RP (computed from Gumbel fit on annual maxima),
Percentile thresholds Q_th	95^{th}-, 98^{th}-, 99^{th}-\% (from the whole daily time series)	95^{th}-, 98^{th}-, 99^{th}-\% (from the whole daily time series)
Threshold–calculation timeframe	01/01/1980–31/12/2023	01/01/1980–31/12/2023

Flood events were defined using exceedances of both return period thresholds (1.5-, 2-, 5-, and 10-year return periods) and percentile-based thresholds (i.e. 95th, 98th, and 99th percentile). Table 1 outlines the used thresholds and analysis timeframes. Return periods were estimated using a Gumbel fit on annual maxima, while percentiles were calculated from the full discharge record. Exceedances within a 10-day action lifetime window were merged into single events. This resulted in datasets of modelled, observed and impact events, whose sample sizes are listed in Table B3.

Forecasted events were compared to ground truth events on both temporal and spatial overlap. We report two standard skill metrics: the probability of detection (POD) and the false alarm ratio (FAR). Following Duque et al. (2023), a POD > 0.6 and a FAR < 0.3 are generally considered as "good'', and a POD > 0.5 and FAR < 0.5 as "acceptable".

4. Results

Forecast skill was assessed against two ground truths: river discharge observations in Section~4.1 and reported impact events in Section~4.2.

4.1 Skill analysis against discharge observations

To give an initial impression of the model's behaviour relative to ground truth data over time, Figure~5 shows a sample of observation discharges and corresponding impact data events with corresponding predicted discharges of GloFAS v3.0, GloFAS v4.0, and Google Flood Hub. The three models reproduced seasonal discharge patterns across years. The plot also illustrates the limited correspondence between recorded impact events and periods of high discharge. Impact data results will be discussed in more detail in Section~4.2.

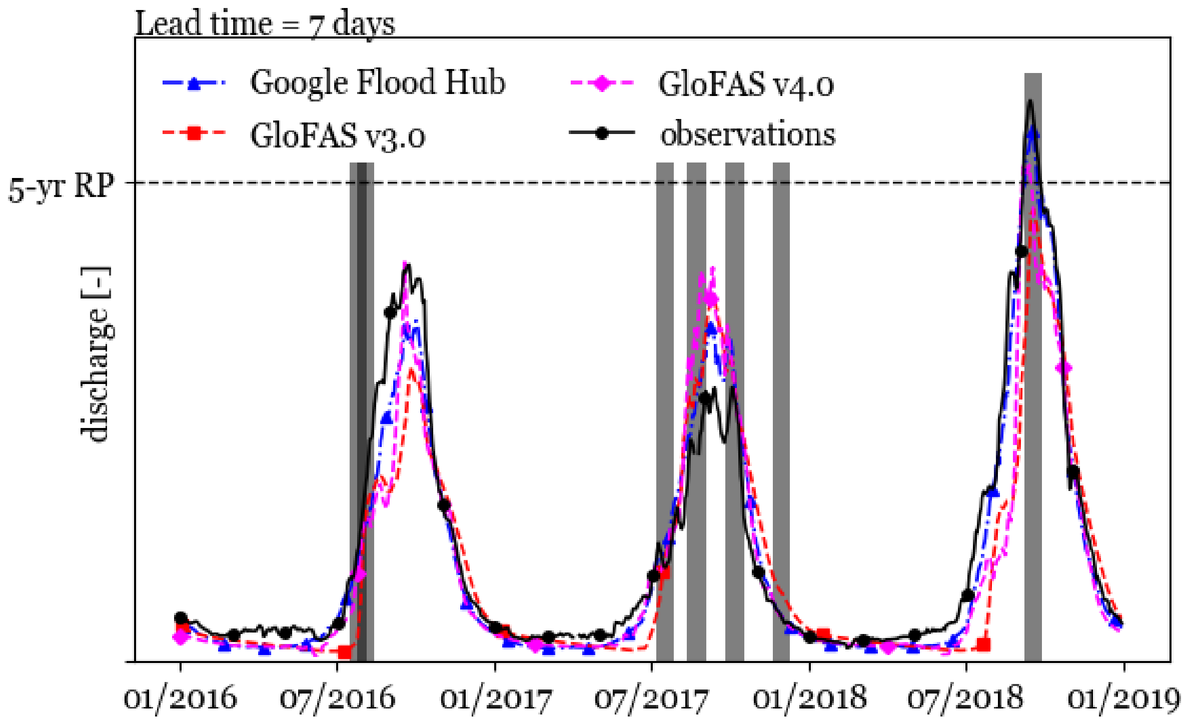

Figure 5: Threshold-normalised timeseries plot for Bamako showing Google Flood Hub and GloFAS forecasts against observations and impact events. Vertical grey bars indicate impact events and include action lifetimes of 10 days.

Figure~6 shows mean POD over all observation stations as function of threshold for a 7-day lead time. GloFAS v4.0 detects more percentile-based floods than GFH and scores a "Good'' POD, but GloFAS v4.0's POD decreases for return-period thresholds, where GFH detects more floods and scores a "Good'' POD. Figure~7 shows the same set-up for FAR. GFH produces more false alarms than GloFAS v4.0 and performs poorly with a FAR of around 0.8 over thresholds. GloFAS v4.0's FAR is more stable, around 0.5 over thresholds (with the exception of the 10-year return period threshold), scoring an "Acceptable'' FAR. Combining POD and FAR of both models, we see GFH favours higher detection at the cost of more false alarms, while GloFAS v4.0 offers a more balanced trade-off. Furthermore, across thresholds where both versions are available, GloFAS v4.0 outperformed GloFAS v3.0 on POD and FAR, supporting the use of GloFAS v4.0 in the analysis.

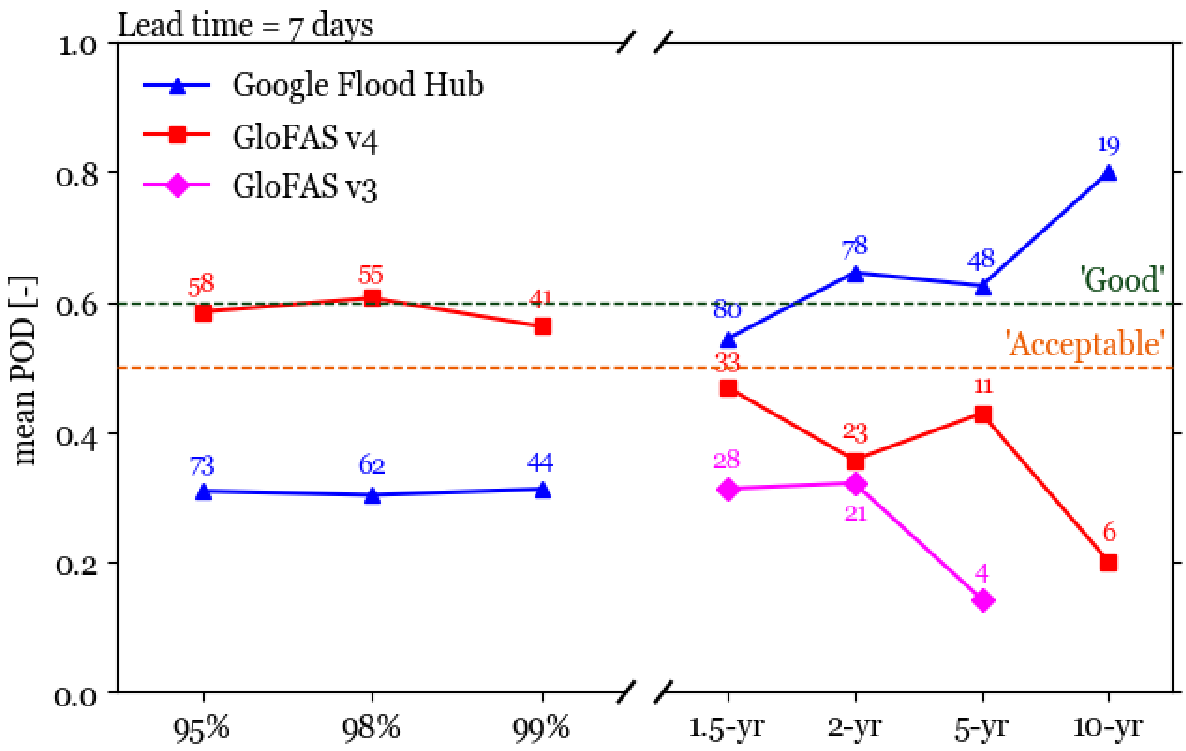

Figure 6: Mean probability of detection (POD) score over all stations as a function of threshold (with discharge observations as ground truth) for 7-day lead time. Sample sizes are indicated above (or below) datapoints. GloFAS v3.0 results for percentile thresholds were not calculated, while for its 10-yr return period, $n = 0$.

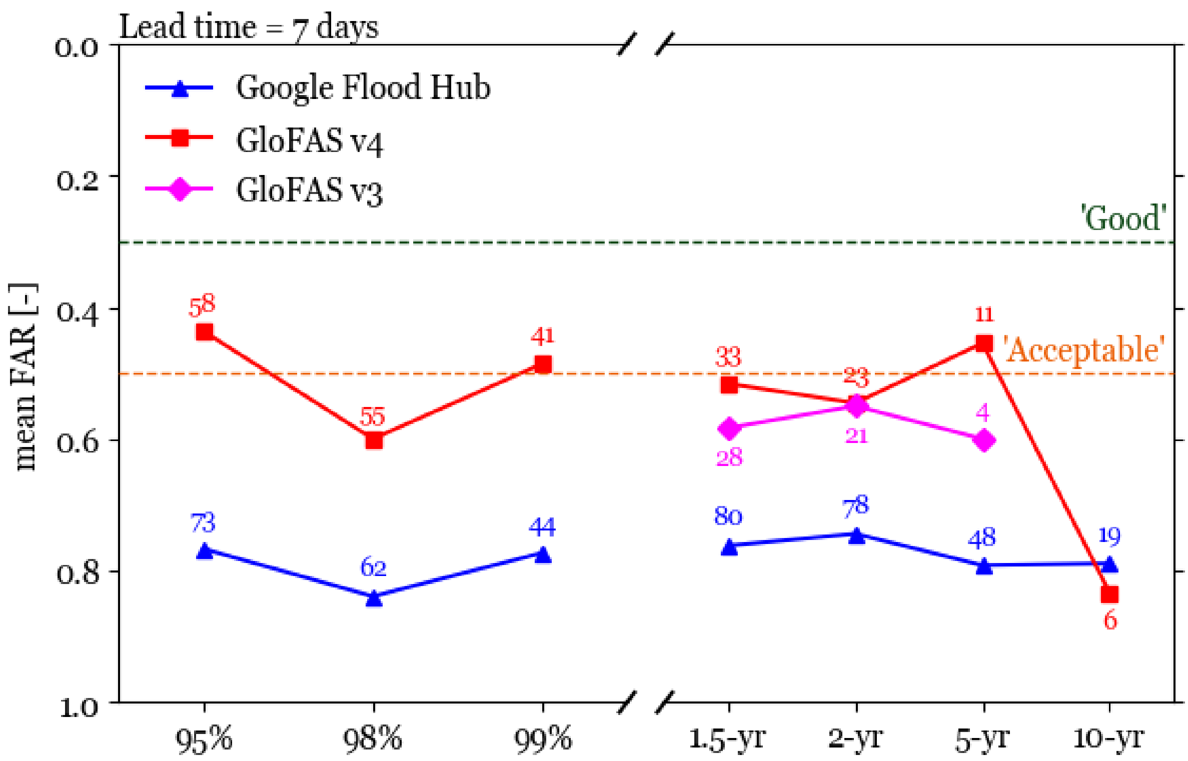

Figure 7: Mean false alarm ratio (FAR) score over all stations as a function of threshold (with discharge observations as ground truth) for 7-day lead time. Sample sizes are indicated above (or below) datapoints. GloFAS v3.0 results for percentile thresholds were not calculated, while for its 10-yr return period, $n = 0$.

Table 2: Performance of PTM, for different river gauges and lead time using a 95th percentile flood threshold over the period between 2016 and 2019 (up to but not including).

Station	**Lead time (days)**	**POD 95th %**	**FAR 95th %**	**# floods predicted**	**# floods observed**
Bamako	4	1	0.5	4	2
Koulikoro	1	0	0	0	1

Table 2 shows the performance of the PTM. It achieves a good performance at a 4-day lead time (POD = 1.0, FAR = 0.5, based on four predicted floods), which we use as a benchmark when assessing whether GloFAS and GFH can extend Mali's current trigger model in lead time and spatial coverage.

Figures~8~and~9 show, for each model and lead time, the mean POD and FAR scores averaged over all stations included in the analysis, as well as the distribution of the corresponding threshold-specific mean scores. The violin plots summarise the spread across thresholds, and the bolded lines indicate the mean per model. For the POD, we see it decreases only slightly with increasing lead time for the three models, while FAR remains constant or increases just slightly with increasing lead time. Consistent with Figure~6~and~7, GFH has the highest mean POD but also the highest FAR at all lead times, indicating many false alarms. GloFAS v4.0's scores remain more balanced, with an "Acceptable'' POD and FAR. Furthermore, of the three models, GFH shows the most variability between thresholds. Overall, extending the lead time from 4 to 7 days has little effect on forecast skill against discharge observations, suggesting GloFAS and GFH can provide actionable guidance beyond the current operational window.

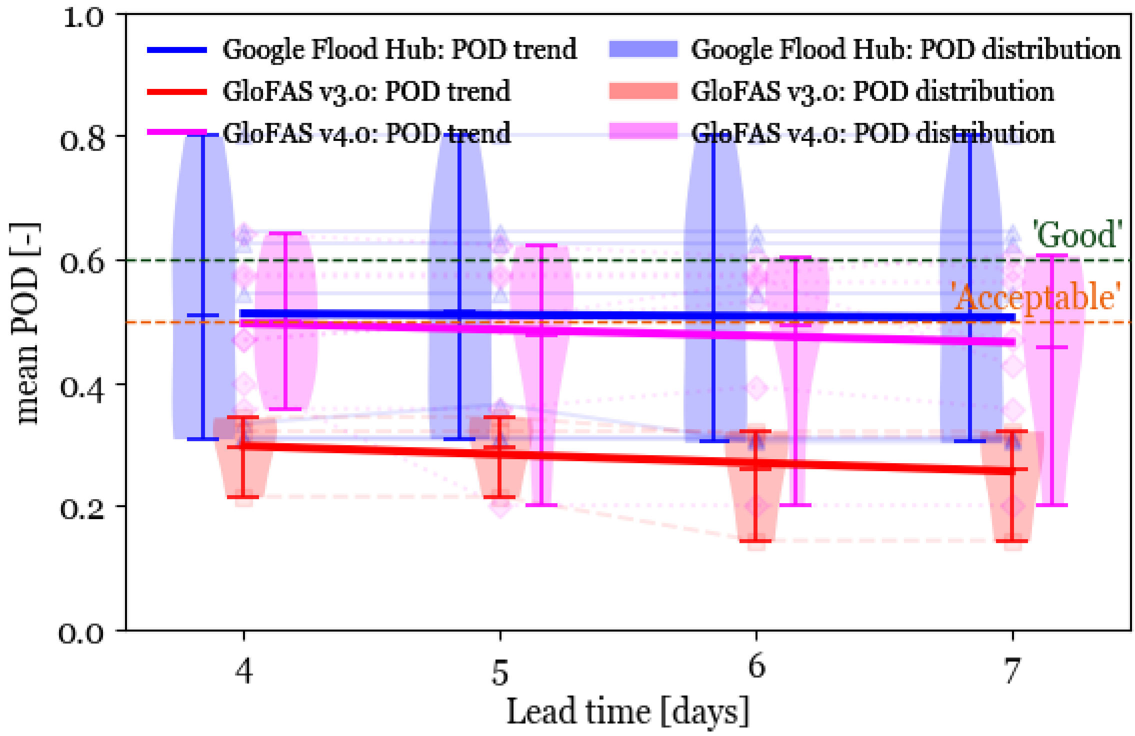

Figure 8: Mean probability of detection (POD) score, averaged over all stations, and the distribution of these threshold-specific (95th-, 98th-, 99th-percentile \& 1.5-yr, 2-yr, 5-yr, 10-yr return period) mean scores as a function of lead time for Google Flood Hub, GloFAS v3.0, and GloFAS v4.0. Solid bold lines depict the trend in mean POD across all thresholds per model, whereas faint lines in the background depict all thresholds individually. Dashed horizontal lines mark reference levels for forecast performance.

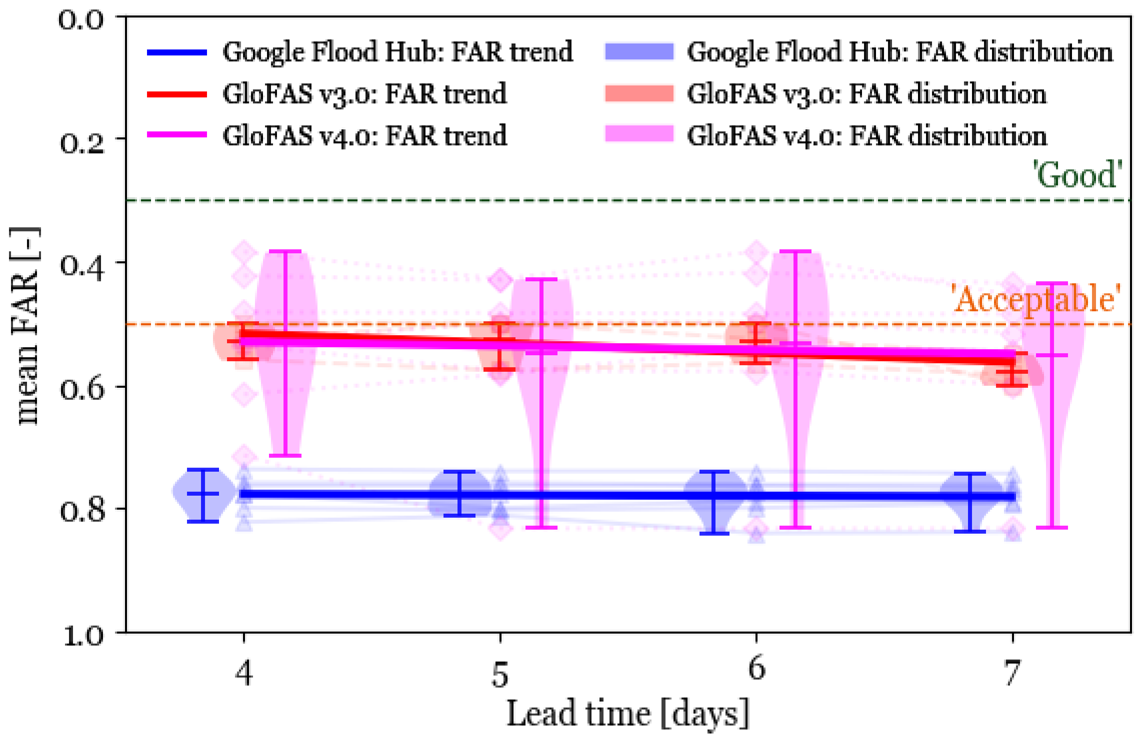

Figure 9: Mean false alarm ratio (FAR) score, averaged over all stations, and the distribution of these threshold-specific (95th-, 98th-, 99th-percentile \& 1.5-yr, 2-yr, 5-yr,

10-yr return period) mean scores as a function of lead time for Google Flood Hub, GloFAS v3.0, and GloFAS v4.0. Solid bold lines depict the trend in mean POD across all thresholds per model, whereas faint lines in the background depict all thresholds individually. Dashed horizontal lines mark reference levels for forecast performance.

Figure 10 shows per-station prediction performance of GloFAS v4.0 and GFH for 95th percentile floods at 7-day lead time. The top two images, A and B, show GloFAS, while the bottom two images, C and D, show GFH. This plot helps assess whether the current operational spatial coverage can be extended to additional regions. Consistent with Figures~6~and~7, GloFAS performs well for this threshold. It attains 1.0 POD and close to 0.0 FAR for the Koulikoro and Bamako stations, and has some combinations of ``Good'' POD with ``Good'' FAR. GFH scores lower than GloFAS over most stations, but outperforms it at Bougouni. At stations Dire, Gao, and Bafing Makana, both models performed poorly.

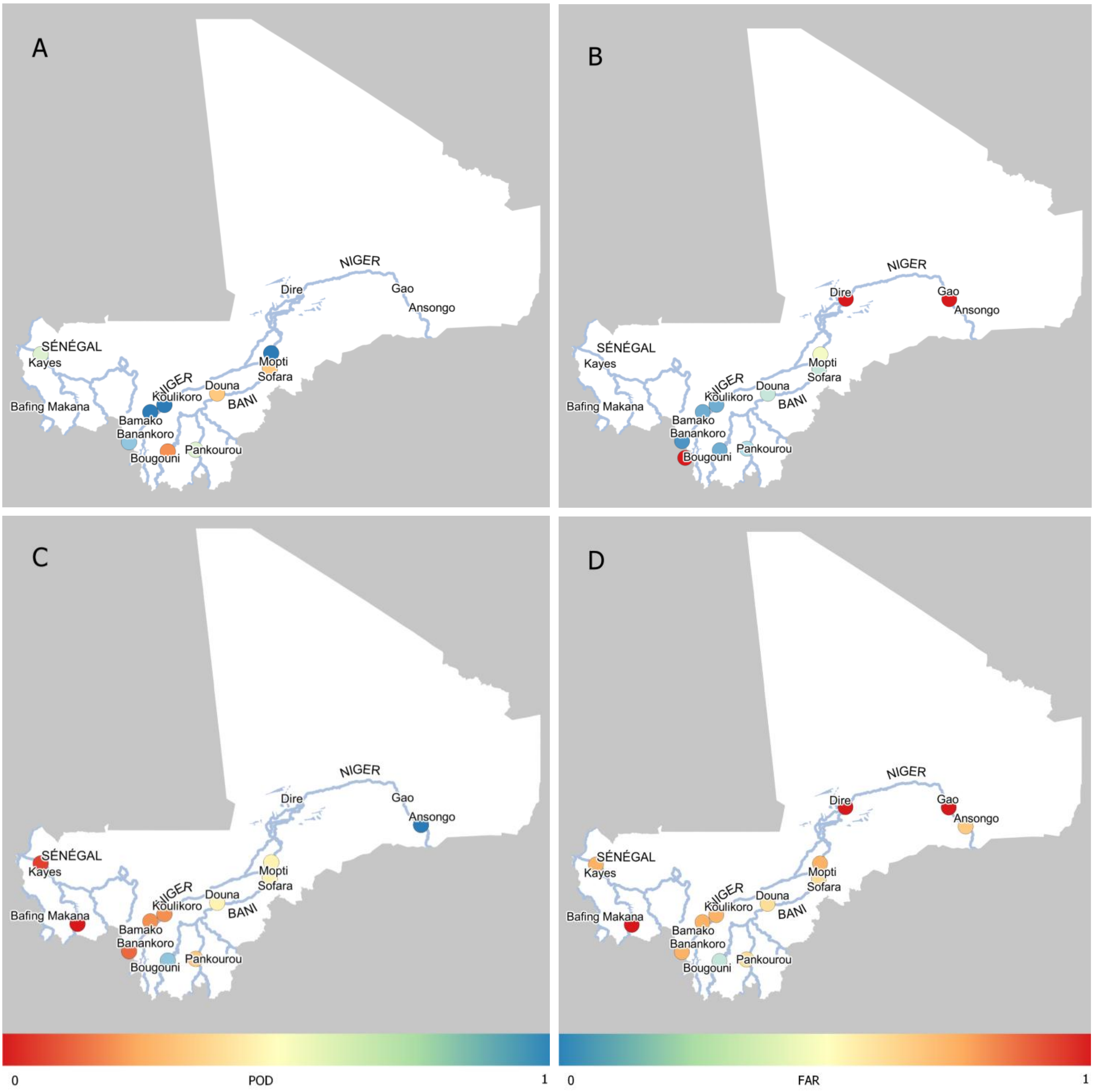

Figure 10: Per-station performance of GloFAS (A: POD; B: FAR) and Google Flood Hub (C: POD; D: FAR) against discharge observations for 95th percentile floods and a 7-day lead time.

4.2 Skill analysis against impact data

Figure~11 shows the per-district performance of 7-day lead time GloFAS forecasts against impact data taken with a 5-year return period threshold. Figure~12 shows the same set-up for Google Flood Hub. In most districts, the models score a 0.0 POD and a 1.0 FAR, meaning the forecasts and ground truths had no overlap. GloFAS did achieve moderate POD (in the range of 0.3–0.4) with few false alarms in the Southern districts Tominian, San, and Bla. Google Flood Hub had a 0.5 POD and 0.0 FAR for the Djenné district.

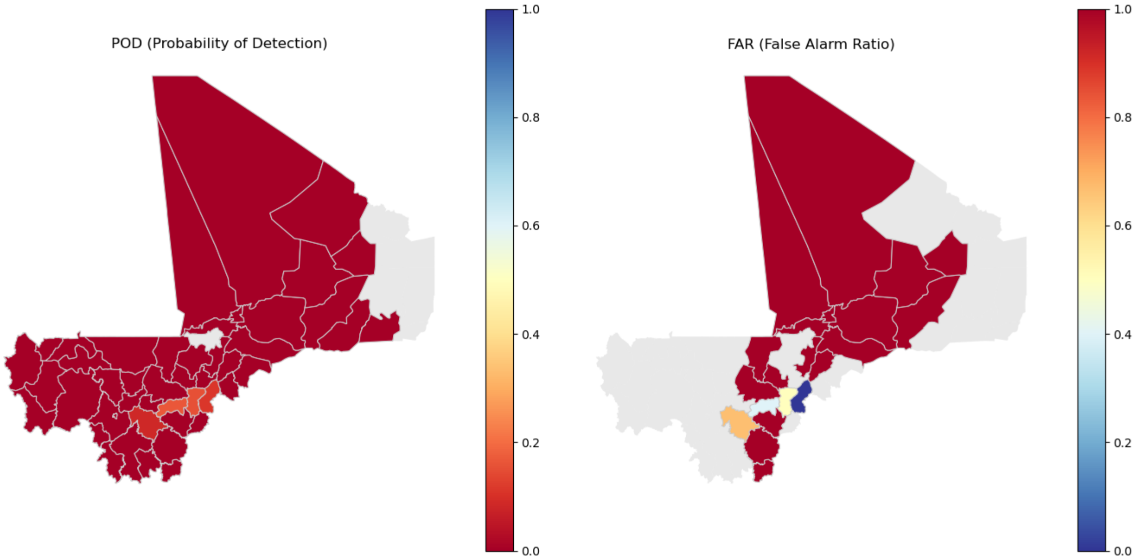

Figure 11: Per-district performance of GloFAS (left: POD; right: FAR) against impact data for a lead time of 7 days and a 5-year return period threshold.

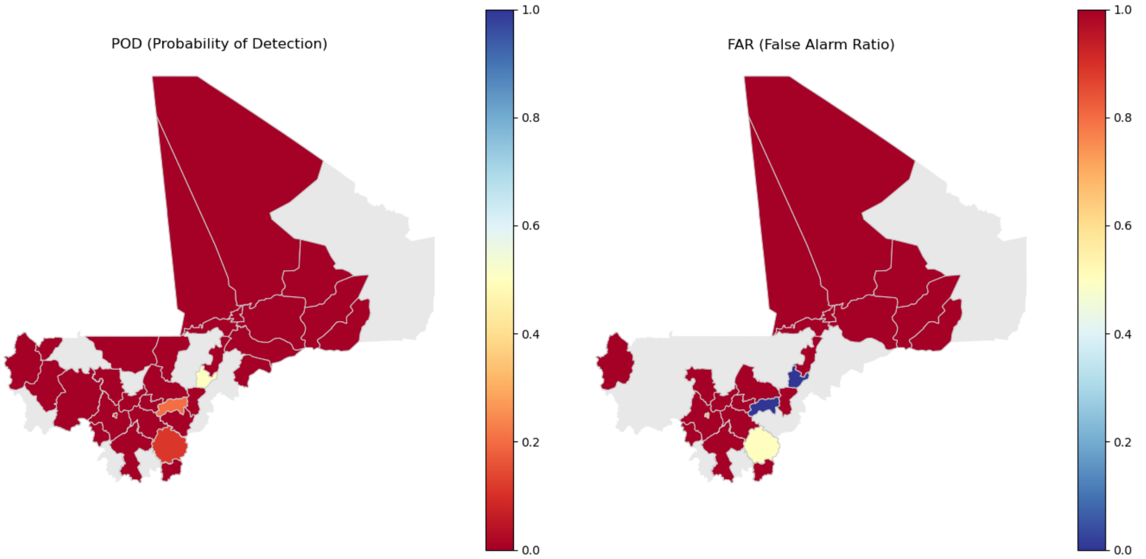

Figure 12: Per-district performance of Google Flood Hub (left: POD; right: FAR) against impact data for a lead time of 7 days and a 5-year return period threshold.

Figure~13 shows the per-district performance of 7-day lead time GloFAS forecasts against impact data taken with a 1.5-year return period threshold. Figure~14 shows the same set-up for Google Flood Hub. While most districts still get 0.0 POD in conjunction with 1.0 FAR, performance has increased somewhat compared to the 5-year return period threshold, explained by the increase in threshold exceedances (and thus predicted events) with a lower threshold. GloFAS' scores improved the most with the change in threshold. Especially regions around the Niger river in the South, GloFAS shows improvements, with some improvements around the Senegal river, in Koulikoro, specifically Nara, as well. For Google Flood Hub, Figure~14, the districts Douentza and Koro in Mopti and Yelimane in Kayes showed improvements. However, for both thresholds, both models had no correctly predicted floods in the North of Mali.

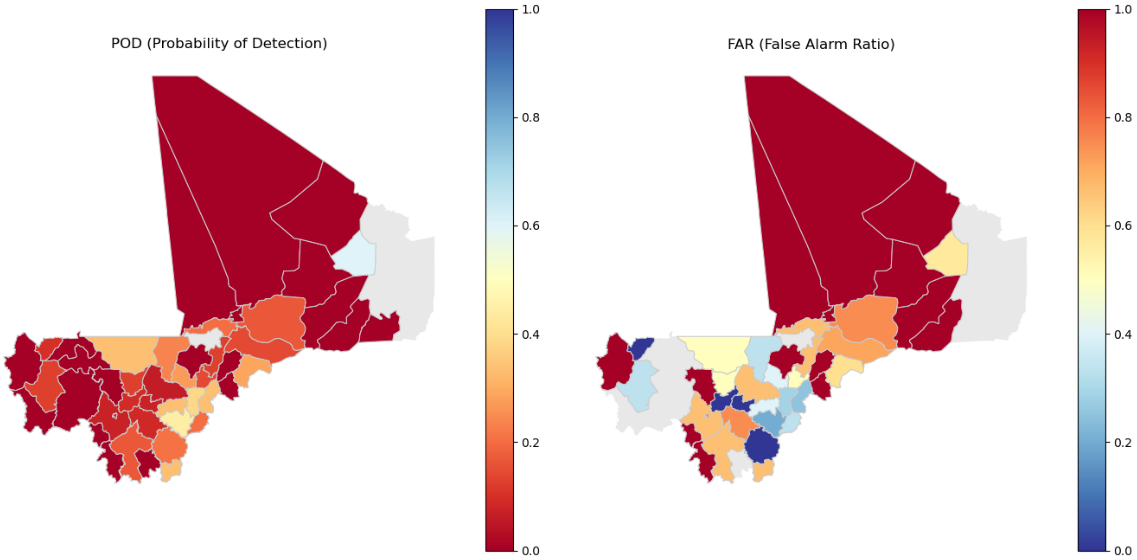

Figure 13: Per-district performance of GloFAS (left: POD; right: FAR) against impact data for a lead time of 7 days and a 1.5-year return period threshold.

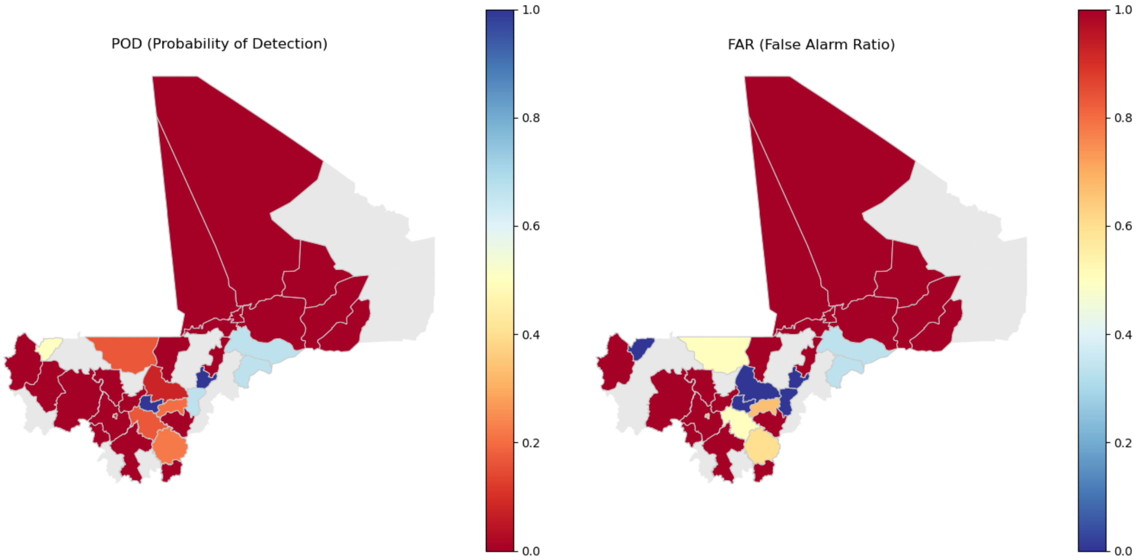

Figure 14: Per-district performance of Google Flood Hub (left: POD; right: FAR) against impact data for a lead time of 7 days and a 1.5-year return period threshold.

5. Discussion

This study aimed to address potential improvements of Mali's EWS in a user-centered assessment of GloFAS and GFH. It provides the first systematic comparison of physics-based GloFAS and AI-based GFH flood forecasts against both hydrological and impact-based ground truths in Mali. We examined whether these models could strengthen existing national models by comparing it with ground truth impact data and observational river flow data. In particular, we: (i) assessed the usability of the two ground truths; (ii) assessed the possibility of the current EWS in lead time and spatial coverage; and (iii), more generally, evaluate user-oriented forecast skill across models and contexts.

5.1. Interpretations

First, regarding point (i), the results highlight that the two ground truths differ in their usability for evaluating forecast skill. The station-level discharge observations gave a consistent reference: although it was spatially sparse with few stations and limited to a short period of overlap (2016–2018), it resulted in interpretable metrics. In contrast, the impact data was heterogeneous and inconsistent in time and space and invariant in flood severity. Here, a possible partial cause of the limited overlap of riverine forecasts with the impact data could be the ambiguous inclusion of flash floods into impact data (Mitheu et al., 2023). Illustratively, the 2016 flood in Figure~5 was ultimately identified as a flash flood caused by heavy rainfall rather than a riverine flood (IFRC, 2016). Figure~5 also illustrates the impact events' inconsistency over time, with the events not coinciding with periods of high discharge, which, together with the other deficiencies, led to the low scores described in Section~4.2. While impact data could be a valuable ground truth in theory by directly quantifying impact, its usability is limited by its current quality.

Similar findings have been reported in evaluating GloFAS in African regions (van den Homberg et al., 2022a; Mitheu et al., 2023). Some examples of its flaws are: sparsity caused by under-reporting of impacts; invariance to flood extremity, meaning floods of all severities were compared against predicted floods of varying severity; and inconsistencies in definitions of flood starts and endings across datasets and datapoints. Utilising low-quality impact data can lead to underestimating forecast skill, highlighting the importance of verification with observations (Gall, 2015; van den Homberg et al., 2022a; Mitheu et al., 2023). Overall, the findings suggest that discharge observations are currently the ground truth of choice for impact-based forecast evaluation.

Second, regarding point (ii), the results show that Mali's current trigger model can be extended, both in lead time and spatial coverage. Compared to the 4-day horizon of PTM, GloFAS v4.0 and GFH showed little change in POD and FAR between 4- and 7-day lead times against discharge observations, indicating that increasing the lead time is feasible at well-performing stations without compromising on performance. Spatially, the models' performance showed more variability. Assessment in the Northern regions (Tombouctou, as well as in large parts of Gao and Kidal) was challenging due to the absence of monitoring stations. At the national scale, GloFAS' continuous gridded dataset and GFH's multitude of virtual gauges give access to forecasts over a much larger part of Mali than the few PTM gauges, although performance was weak in some regions and is yet to be validated in others by unavailability of observation data. The higher spatial coverage of the models may also help pinpoint specific communities affected, which is of particular concern for urbanising areas, where flooding leads to significant losses of life and livelihoods (Kam et al., 2024).

Third, regarding point (iii), a user-oriented evaluation of forecast skill shows both systems can be operationally useful for early warnings, though each model needs its own considerations. GFH attains a higher POD for some locations and especially more extreme thresholds, but at the cost of false alarms, i.e. a high FAR. Low FAR values are critical for deployment to avoid unnecessary emergency responses, as these strain the forecast-based financing system and erode trust in EWSs. GloFAS, on the other hand, provides a more favourable balance of ``Good" or near ``Acceptable'' POD combined with ``Acceptable'' FAR. For example, for the 95th percentile threshold results in Figure~10, GloFAS v4.0 was especially favourable in Southern regions, such as Sikasso. Additionally, the long-term free and open availability of GloFAS, which has already led to implementation in other EAPs (Anticipation Hub, 2023), enhances trust in its use for operational triggers. More generally though, both models' performance varied considerably across regions, thresholds, and dimensions of data availability and quality, highlighting the importance of context-specific implementation.

5.2. Strengths and limitations

A limitation of the analysis is that global models like GloFAS and GFH rely on generalized assumptions about infiltration and runoff, which may lead to an underestimation of peak flow predictions in arid regions. In semi-arid regions, flood runoff potentials are generally higher than in more humid areas. In humid environments, soil and vegetation absorb and intercept rainfall, thereby attenuating runoff. Conversely, in arid areas, limited infiltration on bare, crusted surfaces facilitates runoff (Osterkamp & Friedman, 2000; Maref & Seddini, 2018).

Changes in the morphology of the rivers may explain a change in discharge-to-flood relationship over the course of the rainy season. In arid regions especially, heavy rainfall and runoff alter the morphology significantly (Osterkamp & Friedman, 2000). The bankfull capacity of rivers such as Niger and Senegal, particularly their ephemeral sections, can vary significantly between the start and end of the rainy season. At the beginning of the season, rivers are less capable of accommodating water, whereas by the end, their capacity increases.

Setting higher thresholds led to lower sample sizes, limiting model assessment (Mitheu et al, 2023; Hossain et al, 2023). Since bankfull discharge is commonly associated with the 1.5-year return period (Castro & Jackson, 2001), these results are considered most reliable for impact analysis. Results for less frequent floods are less robust due to the limited number of events available for analysis (Hossain et al., 2023). Additionally, performance metrics can be influenced by event frequency, which impacts the relationship between flood thresholds and model performance (Baldwin and Kain, 2006). Consequently, higher flood thresholds likely underestimate the models' performance skill.

Beyond these hydrological considerations, AI-based forecasting brings strengths and weaknesses. Recent AI weather models (e.g. ECMWF's AIFS (Lang et al., 2024)) already match or outperform traditional numerical models, while being much faster and cheaper to run. As similar architectures are applied to hydrology, AI-based flood forecasts are likely to become increasingly relevant, either by rivaling or surpassing physics-based systems or, for example, through hybrid systems that combine physics and machine learning. Also, GFH's ability to generalise to ungauged, data-scarce catchments (Kratzert et al., 2019) is particularly useful for countries like Mali where only few rivers are monitored (Nearing et al., 2024); that also means forecasts are hardest to verify precisely where they are most needed. Furthermore, as trained AI models can be relatively cheap to run, it can change how (humanitarian) decision-makers interact with models and data. For example, ECMWF's concept of ``forecasts-in-a-box'' allows users to run models locally, finetuned to their needs (WMO, 2025). However, because AI models learn mainly from historical data, their performance is theoretically least reliable for extreme (possibly out-of-distribution) flood situations, which underlines the importance of independent evaluation. In addition, AI models' black-box nature can undermine user trust (Ribeiro et al., 2016).

5.3. Recommendations

Multiple recommendations to improve impact-based forecasting can be made. Firstly, impact data quality can be enhanced by verification through different sources, for instance satellite imagery. Satellite imagery enhances flood impact data by providing flood extent information, even in data-sparse regions. This would help differentiate the currently used severity-agnostic impact events, which limit the impact data-analysis significantly. Moreover, additionally overlaying satellite-derived flood maps with population and infrastructure data can further enhance the precision of impact assessments (Revilla-Romero et al., 2015).

Secondly, flood extent maps better represent actual flood impacts by accounting for flooding processes rather than relying solely on extreme discharge values. GloFAS's inability to model water exiting river channels when discharge exceeds bankfull capacity, limits its ability to fully represent flood impact on communities (Alfieri et al., 2013; Riedel et al., 2024). To address these limitations, Riedel et al. (2024) models the flood footprint by interpolating discharge probabilities with flood hazard maps. Integrating GloFAS could provide more spatially accurate flood impact predictions. This method is computationally efficient compared to a full tile composite matching as shown by Dottori et al. (2016). In addition, complementing impact-based forecasting models with local knowledge-based approaches that leverage stakeholder expertise and historical knowledge, contextualizes forecasts into real-world scenarios (Bucherie et al., 2022; Sakic Trogrlic et al., 2019). As such, combined methodologies can bridge the gap between hydro-meteorological forecasts and actionable, localized warnings that ultimately improve resilience to hazards (Harrison et al., 2022).

The use of both GloFAS and GFH for specific regions and stations could enhance their effectiveness as trigger models. A complementary implementation—where early actions are triggered only when both models consistently indicate high discharge levels—may help reduce false alarms while maintaining a high probability of detection for likely and impactful events.

6. Conclusion

The user-centred evaluation of GloFAS and GFH indicates that Mali's current trigger model can be extended, both in lead time and spatial coverage. Observational data was found reliable, though impact data in Mali needs improvement for reliable forecast skill assessment. Where both GloFAS and GFH can be operationally useful, they have different strengths: GFH detects more events at the expense of also having more false alarms, while GloFAS offers a more balanced skill profile. Overall, performance differed between regions. Limitations of the models include the underestimation of river flows in arid areas and the inability to fully capture the process of flooding, especially in urban settings. Recommendations include complementary model use, improving impact data quality, and the adoption of a more spatially explicit flood forecasting approach.

Data and code availability

The Global Flood Awareness System (GloFAS) reforecast data are available through the Copernicus Emergency Management Service Early Warning Data Store (EWDS) at https://ewds.climate.copernicus.eu/datasets/cems-glofas-reforecast. Google Runoff Reanalysis & Reforecast dataset (GRRR) are available through Google Research (2024) at https://sites.research.google/gr/floodforecasting/resources/; its metadata were retrieved via private API and can be accessed upon request. The river flow observations in Mali are available for this study under a special non-disclosure agreement with the Direction Nationale de l'Hydraulique (DNH-Mali) via the Croix-Rouge Malienne, and are not publicly accessible over the period used in the study. Researchers can request access to DNH-Mali. The metadata of the river gauge stations considered in this study, as well as historical hydrological observations (for earlier periods) are also provided by the Global Runoff Data Centre (GRDC; https://grdc.bafg.de/data/data_portal/). Impact data are available through the sources listed in Appendix~A, and the data gathered by applying a text-mining algorithm to newspaper articles is available upon request. The code used for processing impact data is available at: https://github.com/rodekruis/disaster-impact-data-analysis.git. Scripts for GloFAS and Google Flood Hub analysis can be found in this repository: https://github.com/rodekruis/river-flood-data-analysis.

References

Aich, V., Liersch, S., Vetter, T., Fournet, S., Andersson, J. C. M., Calmanti, S., van Weert, F. H. A., Hattermann, F. F., & Paton, E. N. (2016a). Flood projections within the Niger River Basin under future land use and climate change. *Science of the Total Environment, 562*, 666–677. https://doi.org/10.1016/j.scitotenv.2016.04.021

Aich, V., Koné, B., Hattermann, F. F., & Paton, E. N. (2016b). Time series analysis of floods across the Niger River Basin. *Water, 8*(4), 165. https://doi.org/10.3390/w8040165

Alfieri, L., Burek, P., Dutra, E., Krzeminski, B., Muraro, D., Thielen, J., & Pappenberger, F. (2013). Glofas: global ensemble streamflow forecasting and flood early warning. *Hydrology and Earth System Sciences, 17*(3), 1161–1175. doi: 10.5194/hess-17-1161-2013

Andersen, J., Refsgaard, J. C., & Jensen, K. H. (2001). Distributed hydrological modelling of the Senegal river basin — model construction and validation. *Journal of Hydrology, 247*(3), 200–214. doi: 10.1016/S0022-1694(01)00384-5

Anticipation Hub. (2023). *EAP activation report: Zambia floods*. Anticipation Hub. (2023). *EAP activation report: Zambia floods*. https://www.anticipation-hub.org/Documents/EAPs/EAP_Activation_Report_Zambia_Floods.pdf

Baldwin, M. E., & Kain, J. S. (2006). Sensitivity of several performance measures to displacement error, bias, and event frequency. *Weather and Forecasting, 21*(4), 636–648. doi: 10.1175/WAF933.1

Bucherie, A., Werner, M., van den Homberg, M., & Tembo, S. (2022). Flash flood warnings in context: combining local knowledge and large-scale hydro-meteorological patterns. Natural Hazards and Earth System Sciences, 22(2), 461-480.

Castro, J. M., & Jackson, P. L. (2001). Bankfull discharge recurrence intervals and regional hydraulic geometry relationships: Patterns in the Pacific Northwest, USA. *JAWRA Journal of the American Water Resources Association, 37*(5), 1249–1262. doi: 10.1111/j.1752-1688.2001.tb03636.x

Cohen, D. (2024, November 11). *An improved flood forecasting AI model, trained and evaluated globally*. Google Research Blog. URL: https://research.google/blog/a-flood-forecasting-ai-model-trained-and-evaluated-globally/. (Accessed February 3rd, 2025.)

Coughlan de Perez, E., van den Hurk, B., van Aalst, M. K., Amuron, I., Bamanya, D., Hauser, T., ... Zsoter, E. (2016). Action-based flood forecasting for triggering humanitarian action. *Hydrology and Earth System Sciences, 20*(9), 3549–3560. doi: 10.5194/hess-20-3549-2016

Croix-Rouge Malienne, I., Direction Nationale de l'Hydraulique. (2023). Funding based on forecasts - early action protocol river floods Mali.

De Filippis, T., Rocchi, L., Massazza, G., Pezzoli, A., Rosso, M., Housseini Ibrahim, M., & Tarchiani, V. (2022). Hydrological web services for operational flood risk monitoring and forecasting at local scale in Niger. *ISPRS International Journal of Geo-Information, 11*(4). doi: 10.3390/ijgi11040236

DNH. (2019). Water levels and discharges of stations along the Niger in Mali.

Dottori, F., Salamon, P., Bianchi, A., Alfieri, L., Hirpa, F. A., & Feyen, L. (2016). Development and evaluation of a framework for global flood hazard mapping. *Advances in Water Resources, 94*, 87–102. doi: 10.1016/j.advwatres.2016.05.002

Duque, L.-F., O'Connell, E., & O'Donnell, G. (2023). A Monte Carlo simulation and sensitivity analysis framework demonstrating the advantages of probabilistic forecasting over deterministic forecasting in terms of flood warning reliability. *Journal of Hydrology, 619*, 129340.

Additionally, the publicly available Google Runoff Reanalysis & Reforecast dataset (GRRR), which contains reforecasts for 2016–2022 and reanalyses for 1980–2024, facilitates historical analysis of flood forecasting accuracy.

Gall, M. (2015). The suitability of disaster loss databases to measure loss and damage from climate change. International Journal of Global Warming, 8(2), 170-190.

Fofana, M., Adounkpe, J., Dotse, S. Q., Bokar, H., Limantol, A. M., Hounkpe, J., ... & Toure, A. (2023). Flood forecasting and warning system: a survey of models and their applications in West Africa. American Journal of Climate Change, 12(1), 1-20.

Google Research. (2024). *Google Runoff Reanalysis & Reforecast (GRRR) dataset* [Data set]. Retrieved from https://sites.research.google/gr/floodforecasting/resources/. (Accessed February 7th, 2025.)

Gumbel, E. J. (1958). Statistics of Extremes.

Harrigan, S., Zoster, E., Cloke, H., Salamon, P., & Prudhomme, C. (2023). Daily ensemble river discharge reforecasts and real-time forecasts from the operational Global Flood Awareness System. Hydrol. Earth Syst. Sci., 27, 1–19, https://doi.org/10.5194/hess-27-1-2023

Harrison, S. E., Potter, S. H., Prasanna, R., Doyle, E. E., & Johnston, D. (2022). Identifying the impact-related data uses and gaps for hydrometeorological impact forecasts and warnings. *Weather, Climate, and Society, 14*(1), 155–176.

Hirabayashi, Y., Mahendran, R., Koirala, S., Konoshima, L., Yamazaki, D., Watanabe, S., Hyungjun, K., Kanae, S. (2013). Global flood risk under climate change. *Nature Climate Change, 3*(9), 816–821. doi: 10.1038/nclimate1911

Hossain, S., Cloke, H. L., Ficchì, A., Gupta, H., Speight, L., Hassan, A., & Stephens, E. M. (2023). A decision-led evaluation approach for flood forecasting system developments: An application to the Global Flood Awareness System in Bangladesh. *Journal of Flood Risk Management, e12959.*

IFRC, FbF Practitioners Manual, Chapter 6, Develop a trigger system. https://manual.forecast-based-financing.org/en/chapter/06-develop-a-trigger-system/, 2025. (Accessed October 25th, 2025.)

IFRC (2016). *Emergency Plan of Action (EPoA): Mali floods (DREF operation no. MDRML012)*. accessed through: https://reliefweb.int/report/mali/mali-floods-emergency-plan-action-fund-n-mdrml012

Kan, G., He, X., Ding, L., Li, J., Liang, K., & Hong, Y. (2017). Study on applicability of conceptual hydrological models for flood forecasting in humid, semi-humid semi-arid, and arid basins in China. *Water, 9*(10), 719.

Kiptum, A., Antonarakis, A. S., Todd, M. C., & Guigma, K. (2024). Characteristics, drivers, and predictability of flood events in the Tana River Basin, Kenya. *Journal of Hydrology: Regional Studies, 53*, 101748. doi: 10.1016/j.ejrh.2024.101748

Kousky, C., Ritchie, L., Tierney, K., Lingle, B., 2019. Return on investment analysis and its applicability to community disaster preparedness activities: Calculating costs and returns. Int. J. Disaster Risk Reduct. 41, 101296. https://doi.org/10.1016/J.IJDRR.2019.101296

Kratzert, F., Klotz, D., Herrnegger, M., Sampson, A. K., Hochreiter, S., & Nearing, G. S. (2019). Toward improved predictions in ungauged basins: Exploiting the power of machine learning. *Water Resources Research*, *55*(12), 11344-11354.

Kratzert, F., Nearing, G., Addor, N., Erickson, T., Gauch, M., Gilon, O., ... & Matias, Y. (2023). Caravan-A global community dataset for large-sample hydrology. *Scientific Data*, *10*(1), 61.

Lam, R., Sanchez-Gonzalez, A., Willson, M., Wirnsberger, P., Fortunato, M., Alet, F., ... & Battaglia, P. (2023). Learning skillful medium-range global weather forecasting. *Science*, *382*(6677), 1416-1421.

Lang, S., Alexe, M., Chantry, M., Dramsch, J., Pinault, F., Raoult, B., ... & Rabier, F. (2024). AIFS--ECMWF's data-driven forecasting system. arXiv preprint arXiv:2406.01465.

Lehner, B., Grill G. (2013). Global river hydrography and network routing: baseline data and new approaches to study the world's large river systems. Hydrological Processes, 27(15): 2171–2186. https://doi.org/10.1002/hyp.9740

Liersch, S., Cools, J., Koné, B., Koch, H., Diallo, M., Reinhardt, J., Fournet, S., Aich, V., & Hattermann, F. F. (2013). Vulnerability of rice production in the Inner Niger Delta to water resources management under climate variability and change. ***Environmental Science & Policy, 34***, 18–33. https://doi.org/10.1016/j.envsci.2012.10.014

Linke, S., Lehner, B., Ouellet Dallaire, C., Ariwi, J., Grill, G., Anand, M., Beames, P., Burchard-Levine, V., Maxwell, S., Moidu, H., Tan, F., Thieme, M. (2019). Global hydro-environmental sub-basin and river reach characteristics at high spatial resolution. Scientific Data 6: 283. doi: https://doi.org/10.1038/s41597-019-0300-6

Loveday, N., Taggart, R., & Khanarmuei, M. (2024). A user-focused approach to evaluating probabilistic and categorical forecasts. *Weather and Forecasting*.

Maref, N., & Seddini, A. (2018). Modeling of flood generation in semi-arid catchment using a spatially distributed model: Case of study Wadi Mekerra catchment (northwest Algeria). *Arabian Journal of Geosciences, 11*, 1–15.

Matthews, G., Baugh, C., Barnard, C., Carton De Wiart, C., Colonese, J., Grimaldi, S., ... Prudhomme, C. (2025). Chapter 15 - On the operational implementation of the global flood awareness system (GloFAS). In T. E. Adams, C. Gangodagamage, & T. C. Pagano (Eds.), *Flood Forecasting (Second Edition)* (pp. 299–350). Academic Press. doi: 10.1016/B978-0-443-14009-9.00014-6

Merz, B., Kuhlicke, C., Kunz, M., Pittore, M., Babeyko, A., Bresch, D. N., ... others. (2020). Impact forecasting to support emergency management of natural hazards. *Reviews of Geophysics, 58*(4), e2020RG000704.

Millington, N., Das, S., & Simonovic, S. P. (2011). The comparison of GEV, log-Pearson type 3 and Gumbel distributions in the Upper Thames River watershed under global climate models.

Mitheu, F., Tarnavsky, E., Ficchì, A., Stephens, E., Cornforth, R., & Petty, C. (2023). The utility of impact data in flood forecast verification for anticipatory actions: Case studies from Uganda and Kenya. *Journal of Flood Risk Management, e12911*. doi: 10.1111/jfr3.12911

Muñoz Sabater, J. (2019): ERA5-Land hourly data from 1950 to present. Copernicus Climate Change Service (C3S) Climate Data Store (CDS). DOI: 10.24381/cds.e2161bac

Nauman, C., Anderson, E., Coughlan de Perez, E., Kruczkiewicz, A., McClain, S., Markert, A., Griffin, R., Suarez, P. (2021). Perspectives on flood forecast-based early action and opportunities for Earth observations. *Journal of Applied Remote Sensing, 15*(3), 032002–032002.

Ndiaye, A., Mbaye, M. L., Arnault, J., Camara, M., & Lawin, A. E. (2023). Characterization of extreme rainfall and river discharge over the Senegal River Basin from 1982 to 2021. *Hydrology, 10*(10), 204. https://doi.org/10.3390/hydrology10100204

Nearing, G., Cohen, D., Dube, V., Gauch, M., Gilon, O., Harrigan, S., . . . others (2024). Global prediction of extreme floods in ungauged watersheds. *Nature 627 (8004), 559–563.*

Osterkamp, W., & Friedman, J. (2000). The disparity between extreme rainfall events and rare floods—with emphasis on the semi-arid American West. *Hydrological Processes, 14*(16–17), 2817–2829.

Pagano, T. C., Casati, B., Landman, S., Loveday, N., Taggart, R., Ebert, E. E., ... Noble, C. (2024). Challenges of operational weather forecast verification and evaluation. *Bulletin of the American Meteorological Society, 105*(4), E789–E802. doi: 10.1175/BAMS-D-22-0257.1

Pappenberger, F., Dutra, E., Wetterhall, F., & Cloke, H. L. (2012). Deriving global flood hazard maps of fluvial floods through a physical model cascade. *Hydrology and Earth System Sciences*, *16*(11), 4143-4156.

Prudhomme, C., Zsoter, E., Matthews, G., Melet, A., Grimaldi, S., Zuo, H., ... others. (2024). Global hydrological reanalyses: The value of river discharge information for world-wide downstream applications—the example of the Global Flood Awareness System GloFAS. *Meteorological Applications, 31*(2), e2192.

Rai, R.K., van den Homberg, M.J.C., Ghimire, G.P., McQuistan, C., 2020. Cost-benefit analysis of flood early warning system in the Karnali River Basin of Nepal. Int. J. Disaster Risk Reduct. 47, 101534. https://doi.org/10.1016/J.IJDRR.2020.101534

Rebelo, L.-M., Johnston, R., Hein, T., Weigelhofer, G., D'Haeyer, T., Koné, B., & Cools, J. (2013). Challenges to the integration of wetlands into IWRM: The case of the Inner Niger Delta (Mali) and the Lobau Floodplain (Austria). ***Environmental Science & Policy, 34***, 58–68. https://doi.org/10.1016/j.envsci.2012.11.002

Rentschler, J., Salhab, M., & Jafino, B. A. (2022). Flood exposure and poverty in 188 countries. *Nature communications*, *13*(1), 3527.

Revilla-Romero, B., Hirpa, F. A., Pozo, J. T.-d., Salamon, P., Brakenridge, R., Pappenberger, F., & De Groeve, T. (2015). On the use of global flood forecasts and satellite-derived inundation maps for flood monitoring in data-sparse regions. *Remote Sensing, 7*(11), 15702–15728. doi: 10.3390/rs71115702

Ribeiro, M. T., Singh, S., & Guestrin, C. (2016). "Why Should I Trust You?": Explaining the Predictions of Any Classifier. Proceedings of the 22nd ACM SIGKDD International Conference on Knowledge Discovery and Data Mining, 1135–1144.

Riedel, L., Röösli, T., Vogt, T., & Bresch, D. N. (2024). Fluvial flood inundation and socio-economic impact model based on open data. *Geoscientific Model Development, 17*(13), 5291–5308. doi: 10.5194/gmd-17-5291-2024

Sakho, I., Dupont, JP., Cisse, M.T. et al. Hydrological responses to rainfall variability and dam construction: a case study of the upper Senegal River basin. Environ Earth Sci 76, 253 (2017). https://doi.org/10.1007/s12665-017-6570-4

Sakic Trogrlić, R. , Wright, G. B., Duncan, M. J., van den Homberg, M. J. C., Adeloye, A. J., Mwale, F. D., & Mwafulirwa, J. (2019). Characterising local knowledge across the flood risk management cycle: A case study of Southern Malawi. Sustainability (Switzerland), 11(6). https://doi.org/10.3390/su11061681

Salinas, J. L., Laaha, G., Rogger, M., Parajka, J., Viglione, A., Sivapalan, M., & Blöschl, G. (2013). Comparative assessment of predictions in ungauged basins; part 2: Flood and low flow studies. *Hydrology and Earth System Sciences, 17*(7), 2637–2652. doi: 10.5194/hess-17-2637-2013

Sedhain, S., van den Homberg, M., Teklesadik, A., van Aalst, M., & Kerle, N. (2025). Evaluating impact-based forecasting models for tropical cyclone anticipatory action. International Journal of Disaster Risk Reduction, 105782.

Skidmore, M., Staatz, J., Dembele, N., & Ouédraogo, A. (2016). Population growth, land allocation, and conflict in Mali. *Area Development and Policy, 1*(1), 113–131.

Traoré, P. C. S., Kouressy, M., Vaksmann, M., Tabo, R., Maikano, I., Traoré, S. B., & Cooper, P. (2007). Climate prediction and agriculture: What is different about Sudano-Sahelian West Africa?. In Climate prediction and agriculture: Advances and challenges (pp. 189-203). Berlin, Heidelberg: Springer Berlin Heidelberg.

Van den Homberg, M., Ficchi, A., Phung, P., Sangare, S., Gado Djibo, A., & Kane, C. (2022a). Assessing the riverine flood forecast skill of GloFAS with streamflow observations and impact data: a case study for Mali. In *EGU General Assembly Conference Abstracts* (pp. EGU22-12673).

Van den Homberg, M., Margutti, J., Basar, E., Wagemaker, J., (2022b), Enriching impact data by text mining digital media, UNDRR Global Assessment Report GAR 2022 chapter, https://www.preventionweb.net/publication/enriching-impact-data-mining-digital-media

Wilcox, C., Vischel, T., Panthou, G., Bodian, A., Blanchet, J., Descroix, L., Quantin, G., Cassé, C., Tanimoun, B., & Kone, S. (2018). Trends in hydrological extremes in the Senegal and Niger Rivers. *Journal of Hydrology, 566*, 531–545. https://doi.org/10.1016/j.jhydrol.2018.07.063

World Food Programme (WFP). (2025). WFP's evidence base on anticipatory action 2015–2024. Rome, Italy: World Food Programme. URL: https://www.wfp.org/publications/wfps-evidence-base-anticipatory-action-2015-2024. (Accessed October 29th, 2025.)

World Meteorological Organization (WMO). (2025, June 30). WMO supports Artificial Intelligence forecasting pilot in Africa. World Meteorological Organization News. URL: https://wmo.int/media/news/wmo-supports-artificial-intelligence-forecasting-pilot-africa. (Accessed February 7th, 2025.)

Yue, H., Gebremichael, M., & Nourani, V. (2022). Performance of the global forecast system's medium-range precipitation forecasts in the Niger River Basin using multiple satellite-based products. *Hydrology and Earth System Sciences, 26*(1), 167–181. doi: 10.5194/hess-26-167-2022

Zare, A., Barbier, B., Bologo-Traore, M., Diarra, A., Mahé, G., & Paturel, J.-E. (2017). Climate forecast perception and needs in wetlands: A case study in the Inner Niger Delta in Mali. *Wetlands, 37*(5), 913–923. https://doi.org/10.1007/s13157-017-0926-0

Zeng, N. (2003). Drought in the Sahel. Science, 302(5647), 999-1000.

Appendix A. Data

Table A1: Overview of the sources used for the impact events dataset. The events are sourced from five public repositories and a text mining algorithm applied to news articles (van den Homberg et al., 2022b).

Source	**Source type**	**Temporal coverage**	**Criteria for inclusion**	**Accessibility**
OCHA	Hosting organisation	2002–2022	Unknown	Through Relief: https://reliefweb.int/disasters
DRPC/DGPC Mali	Primary data provider	2017	Unknown	
Desinventar	Data repository	1906–2014	Unknown	https://www.desinventar.net/DesInventar/index.jsp
CatNat		2001–2022	Unknown	https://www.catnat.net/
EMDAT	Data repository	2000–2022	At least ten deaths (including dead and missing). Or at least 100 affected (people affected, injured, or homeless). Or a call for international assistance or an emergency declaration.	Public after registration: https://doc.emdat.be/
Text mining algorithm	Algorithm	2009–2019	Specific location, detailed flood information	Public algorithm

Appendix B. Methodology

The following sections describe the preprocessing of the impact-, observation-, PTM-, GloFAS-, and GFH data into uniform format, the extreme value analysis for defining flood events, and, lastly, the method of comparing and evaluating. Figure~4 visually depicts the data processing pipeline.

B.1. Preprocessing

To analyse the performance of the PTM, GloFAS, and GFH against impact data and discharge observations, all the different data types need to be converted into a uniform format, both temporally and spatially. To classify a flood as being hit (i.e., correctly predicted) or missed in the forecasts, one can transform timeseries data to binary definitions of impact (Harrison et al., 2022). Hence, the uniform format we use is the binary definition of ``flood events”, which are characterised by a specific *\emph{location}* (e.g. a station or within a larger area such as a district) and a certain *\emph{duration}*. While most impact data already follow this event-based format, the timeseries of discharge observations will be transformed to such format by using discharge thresholds.

One important distinction in the flood event analysis is the spatial resolution considered for comparing the model data with impact data and observation data. Since the impact data (introduced in Section 2.4) had to be aggregated at district-level (Mali’s administrative level 2, as explained in the next section), the timeseries data of the different models is aggregated to these districts for suitable comparison. The observation data, on the other hand, is on a station level, offering the opportunity for a more localized comparison. The following sections describe the preprocessing steps for all datasets into their respective formats: impact data to district-level events, observation data to station-level events, and GloFAS and GFH into both.

B.1.1. Impact data

As introduced in Section~2.4, the impact data originate from various sources, with different spatial resolutions. We aggregated the impact data to Mali’s administrative level 2 as current EAPs work on this administrative level. Administrative level 2 is locally called ``cercles”; for consistency, we will refer to them as ``districts” from hereon.

The concatenated dataset shows considerable heterogeneity in multiple dimensions. Through preprocessing, we attempt to derive a common standardised format, aligning with flood forecasts, which have a start and end date, location, and magnitude (corresponding to the return period threshold of choice). Ideally, in addition to location and timing, an indication of flood severity should be included in impact data as well. Unfortunately, the data proved too ambiguous on flood severity, as different datasets handled different qualitative definitions, or missed the dimension entirely; hence we omit this dimension and cannot align impact data with forecasted data in the dimension of flood magnitude.

The process of standardising impact data spatially and temporally follows a few steps. The first step is to subset time and space dimensions and concatenate them, while manually matching properties between datasets. With this in place, after including start and end dates, and, optionally, country, region, district, and municipality identifiers, the following steps are taken: removing completely empty entries; converting encodings; standardising date formats; reconciling naming differences caused by dialects or other local naming variations; taking into account subdistricts that belong to multiple districts; deriving missing or ambiguous identifiers from their sublocations (by creating and inferring from mappings of other available data); discarding non-classifiable left-overs; merging duplicate events, i.e. same-district events with an overlap in dates; excluding events during the dry season—March until end of June—when discharge in rivers is low and we assume events to represent flash floods, not riverine floods; and adding standardised identifiers and coordinates to match with the flood forecasts. This process can be found in more detail in the code repository, see the data availability statement.

Following the conversion of impact events into a uniform format, we filter them on available time and locations in the model data (whose processing of model hydrographs into predicted events is discussed in the following subsections). Since GFH and GloFAS share a common timeframe of 2016–2022, the impact data are filtered to match this period, i.e. data outside the period is discarded. Over space, the impact data is subsetted too, since not all districts have (an adequate amount of) impact events and/or forecasted events. Spatial subsetting is performed dynamically, meaning that the selection of impact events can differ between models. Event selection is performed for multiple reasons, with the goal of isolating events that can test whether a model gets the timing (and, to a much lesser degree, the severity, since impact data do not discriminate flood severity) right of an extreme flood. One reason, for example, is that some districts might not have model events since (i) a model simply does not cover that district or (ii) the district is situated in the desert (i.e. mostly Northern Mali) where a model will not predict large floods. If the impact events would be kept for such situations (which, in case of ``desert districts'' would be relatively small floods regardless), all impact events would be false negatives. Hence, to account for reasons like these and to avoid skewing the results, impact data is only kept for a district if there are model events available within that district. This type of subsetting decreased the amount of impact events by 11%.

Where there can be no predictions for certain impact data, the opposite, where no impact data exist for certain predictions, can happen too. When, for some set of predicted events, no impact data was available in a district for a given calendar year, the predicted events were discarded. This keeps the focus of the analysis on the timing of events and, simultaneously, tries to address the inherent inconsistency of impact data. The inconsistency of impact data can be attributed to many factors, including that when impact data indicate there was a flood (an ``impact''), real impact is not guaranteed, as, primarily, the binary representation of floods hides relevant information, and, e.g. as datasets contain errors and text-mined articles contain ambiguity; or the indiscriminateness of impact data in terms of flood severity, where e.g. a 95th percentile flood is taken be to equal to a flood with a 10-year return period severity; or given the ambiguous inclusion of flash floods into impact data (Mitheu et al., 2023), as opposed to riverine floods; or because impact data are spatially or temporally inconsistent: for example, many impact datasets aggregate damage over broad regions or long periods, so a district may have had no distinct event recorded at the resolution of the analysis or at the specific moment a predicted discharge crosses a threshold of choice. Therefore, by dynamically subsetting, the predicted discharges and impact data are more aligned and their comparability is improved. In the end, the complete procedure resulted in 110 impact events over the 7-year study period, as listed in Table~2 on sample sizes, distributed over 32 included districts with at least one event.

B.1.2. Flood observation data

In continuation of Section~2.4 on the ground truth data, this subsection describes the modifications made to the observation discharge dataset before it can be turned into events. River discharge can at certain places be heavily affected by anthropogenic activity, such as irrigation and regulated lakes and dams. As these activities are not fully considered in the different forecasting models, locations at lakes and dams are excluded from the analysis. The full dataset contains observations from 14 locations (mapped out in Figure~2), and because the station Guelelinkoro falls into this category, the analysis is performed with the remaining 13 stations as ground truth. Section~B.3 describes how the hydrographs of these stations are sampled for event creation.

B.1.3. PTM

We simulated a reanlysis of the PTM that assumes propagation of streamflow through the river netwerk. Observed upstream events were related to downstream river gauges using predefined lag times as in the PTM setup. Observed flood events were first extracted from hydrometric station data based on threshold exceedances. For each identified upstream event, its start and end dates were temporally shifted according to the estimated propagation time to a downstream location. These shifted events represent predicted occurrences at the downstream stations, effectively providing lead-time information. Though there are more streamflow stations in Mali, only five of these are related to eachother in terms of propagation or lag time (see Table B1).

A set of station pairings, as in Table~B1, with corresponding travel times was used to define the flow connectivity and lag between sites. For each pair, the method checks for upstream events and, where present, generates a corresponding downstream event by applying the time lag. The resulting events are then compiled into a single dataset of predicted downstream events with their corresponding impacts.The procedure was repeated across multiple return period thresholds.

Table B1: List of stations where the PTM is adopted, as in the current EAP, and the time in days for discharge to reach the downstream station from the upstream station. The location of stations for which discharge data was available, can be found in Figure~2.

Upstream station	Downstream station	Propagation (lead) time
Banankoro	Bamako	4

Bamako	Koulikoro	1
Koulikoro	Tamani	3
Tamani	Kirango	2
Kirango	Ké-Macina	1

B.1.4. GloFAS

We evaluate the skill of the GloFAS v4.0, using reforecast data which can freely be retrieved from the Copernicus Emergency Management Service Early Warning Data Store (EWDS), using the \texttt{cdsapi} Python library. The dataset provides a gridded modelled river discharge time series, run from 2004 to 2022. The reforecasts are initialised twice weekly with lead times up to 46 days. The raw gridded data and the real world stations can be viewed in Figure~1, in Section~2.3. In locations where river discharge is heavily influenced by human activities such as dam operations or artificial reservoirs, model forecasts may diverge significantly from observed values. Since such anthropogenic factors are not accounted for in the GloFAS model, we exclude affected locations from the analysis. This ensures that model evaluation focuses on areas where discharge is primarily driven by natural hydrological processes.

\textbf{**Zonal aggregation for impact data.**}\quad To evaluate forecast skill with respect to potential impacts, we aggregate modelled discharge values across administrative districts. Within each administrative unit, we calculate the maximum forecasted discharge and compare this value to predefined return period thresholds maps as supplied by GloFAS, which is based on reanalysis data. This comparison is carried out separately for each ensemble member, resulting in a binary exceedance classification. The proportion of ensemble members exceeding the threshold is then used to estimate the probability of a threshold exceedance for each administrative unit. This approach allows us to translate raw discharge forecasts into spatially aggregated indicators of potential flood impact.

Forecasted discharges are compared against both observed river discharge measurements and administrative-level impact thresholds. To ensure a meaningful comparison between the modelled data and in-situ observations, we aligned the river network of GloFAS to the real-world river gauges using upstream area data. Due to spatial mismatches between station coordinates and the coarser model grid, we identified the most representative model location for each station by matching the reported upstream area of the reporting point with the upstream area from the model grid. A search is conducted within a 10-kilometre radius around each river gauge to find the best match, selecting the grid cell with the closest upstream area. This approach ensures that comparisons are made at hydrologically consistent locations, avoiding mismatches due to spatial resolution or topographic inaccuracies

Together, the point-based validation against observed data and the spatially aggregated impact analysis provide a comprehensive assessment of the GloFAS model’s skill in representing both river flow dynamics and potential flood risks at different spatial scales.

B.1.5. Google Flood Hub

To transform GFH’s forecasts into flood events, we use the GRRR reforecast dataset available from 2016 to 2022 (Figure~3) considering different thresholds and lead times. Similar to the case of GloFAS, we transform location-fixed timeseries data to (i) aggregated events per district for the impact data comparison and (ii) station-matched events for the observation data comparison. The discharge thresholds are calculated over the reanalysis data of 1980 to 2023 by fitting an extreme value distribution to annual maxima, as further reported in Section~3.2.

Virtual gauges with a 5-year return period level below \SI{100}{\cubic\metre\per\second} are excluded from the analysis, as we aim to focus on major floods with significant impact, as done in EAPs. For Mali, this excludes 92.5\% of virtual gauges.

\textbf{**Zonal aggregation for impact data.**}\quad Using shape files of administrative units of level 2 in Mali, all virtual gauges are classified into their respective districts so they can be matched with impact data. A caveat here is that virtual gauges are placed on waterbodies, and that waterbodies often form borders between regions. As such, an on-border gauge can arbitrarily fall into one of its nearby districts, while a flood at its location will affect all of its nearby regions. To account for this, we change a gauge's location from a point to a circle with a radius of 5 km, and all regions that overlap are considered a match. This radius-based approach led to 39% more gauge-to-district assignments.

\textbf{**Local aggregation for observation data.**}\quad To aggregate the forecast timeseries at all points assigned to a district, the maximum is taken over all timeseries at every time step, as shown in Figure~B1. The maximum discharge is considered here to focus on the locations experiencing the most extreme water levels consistently for all districts, while simultaneously eliminating the influence of irrelevant low-discharge stations. Alternative aggregations, e.g. using the most upstream gauge in a district or a discharge quantile, could be researched in the future. From these resulting single timeseries per district, events are created as discussed in Section~3.2.

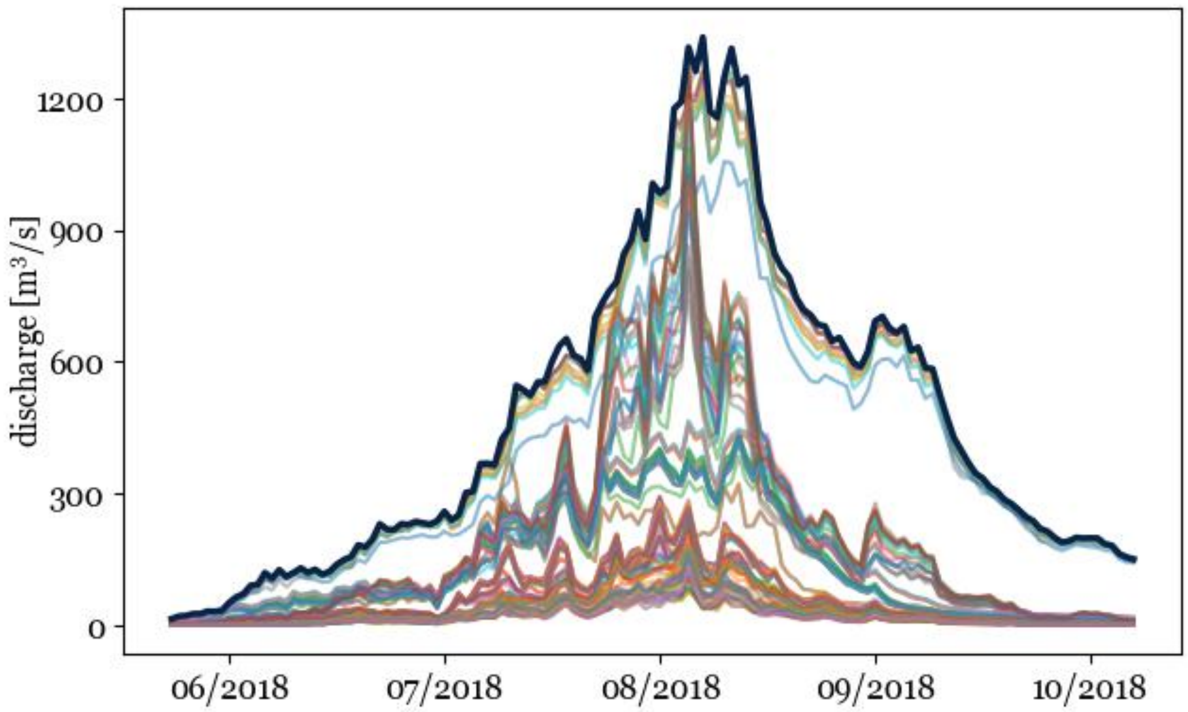

Figure B1: Timeseries plot of all streamflow forecasts at GRRR virtual gauges in one of the Mali districts (Kita) over a 4-month period in 2018 with lead time of 7 days. The dark blue line on top denotes the maximum of all gauges at every time step, visualising the zonal aggregation process.

\textbf{**Local aggregation for observation data.**}\quad For the comparison with observation data from the 13 DNH stations, a point-to-point pairing is performed for all included virtual gauges (which are mapped out in Figure~3). Similar to the DNH-to-GloFAS matching procedure, for GFH we compare upstream areas provided by DNH with drainage areas for virtual stations to construct pairings with approximately the same watershed(s). Note that it is possible for a DNH-station to require the summing of two (or more) virtual gauges, e.g. when the station is located just downstream of a river join.

The procedure is as follows: first, for each station (taken as a one-dimensional point), gather all virtual gauges within a geodesic distance of 10 kilometers. Of those, select the closest ones, with a maximum of three. Then, find a combination of the sample that fits the DNH-station's drainage area with a maximum deviation of 10\%. Finally, manually inspect the found pairings and correct where needed (as the automatic procedure might, for example, select a ` `similar” station in a close but different river). Despite this matching procedure, performance will be limited by differences in the locations and drainage areas of observation data stations and matched virtual gauges.

B.2 Calculating thresholds

Before flood events can be sampled from the GloFAS and GFH timeseries, thresholds Q_{th} need to be determined from the discharge timeseries $Q(t)$. We consider two different methods to determine thresholds: return periods and streamflow percentile thresholds. Return periods are of interest in an operational context and are calculated from annual maxima. Streamflow percentiles are calculated from daily streamflow percentile thresholds. The levels of these thresholds can be found in Table~1. Given that we have a short data record, the percentile-based thresholds are statistically more robust because they use all the available data and not only the tail of our dataset. MacLeod et al. (2021), Hossain et al. (2023) and Mitheu et al. (2023) also use percentile-based thresholds for their GloFAS evaluations. Coughlan de Perez et al., (2016) state that for models like GloFAS that lack local calibration, interpreting absolute discharge values through the lens of anomalies with respect to past discharge distributions can be particularly valuable. Extreme value analyses need long data records to be robust and assume stationarity, which might not be the case. We also do not need to rely on restrictive distributional assumptions as is necessary for the extreme value analysis. Nevertheless, we still include the extreme value analysis because it is sometimes used and preferred in, for example, regulatory context.

B.2.1. Return period thresholds

Statistical analysis of past river discharge data, whether hindcasted or observed, is an established method to relate historical and predicted events (Riedel et al., 2024). Probability of flood occurrence can be expressed via return periods, which quantify how often a discharge value is expected to be exceeded. Because the models come with different return period thresholds, caused by different data, types of fits, and timeframes for the calculations, we recalculate the return period thresholds (as well as the percentile thresholds, discussed next section).

There exists no scientific consensus on the choice of fit for the extreme value analysis. GFH, for instance, employs a Log-Pearson Type III (LP3) fit (Nearing et al., 2024), GloFAS a Gumbel fit (Pappenberger et al., 2012).

For our purposes, the simple yet effective Gumbel fit (Gumbel, E., 1958) with standard calculation methods suffices. Therefore, we also want to calculate return period thresholds for GFH based on the Gumbel fit. GFH return period thresholds are calculated for every gauge by fitting a Gumbel to the annual maxima of the full reanalysis dataset. Furthermore, for districts, return periods are computed on the zonally-aggregated district reanalysis hydrographs in a computationally identical fashion (although alternative methods, such as taking the return period from the most-upstream gauge, could be researched in the future). For the observation data analysis of GFH, this results in per-station datasets with the different thresholds as attributes; for the impact data analysis of GFH, the aggregation procedure followed by extreme value analysis results in per-district datasets with aggregated reforecasted district hydrographs and the thresholds calculated from aggregated reanalysis hydrographs as attributes. Similarly, GloFAS supplies a raster with threshold values as calculated over the reanalysis data.

B.2.2. Streamflow percentile thresholds

For each GFH gauge, daily values from the full reanalysis dataset were ranked, and various percentiles were sampled as thresholds. Similar to the return periods, these thresholds are immediately suitable for the observation data-analysis, and for the impact data-analysis, the thresholds are calculated on the district hydrograph.

Coughlan de Perez et al., (2016) state that for models like GloFAS that lack local calibration, interpreting absolute discharge values through the lens of anomalies with respect to past discharge distributions can be particularly valuable. Accordingly, for discharge values at the reporting points to the hydrological stations, percentiles were calculated through a general extreme value analysis (GEV).

B.3. Sampling modelled and observed events independently

As shown in Figure B2, Mitheu et al. (2023) extend the period of when the trigger is valid by the action lifetime to highlight the usefulness of humanitarian early actions, even when events occur later than forecast. Accordingly, our analysis considers a modelled and observed event as a hit if they occur within a predetermined window of time (i.e., the action lifetime) of each other. Action lifetime is defined as the length of time that the positive impacts of the action will last after the action is implemented. For example, if drains are cleared in a city to reduce potential flooding, the drains may remain sufficiently clear for a few weeks, having a temporary lasting effect (Anticipation Hub, 2025).

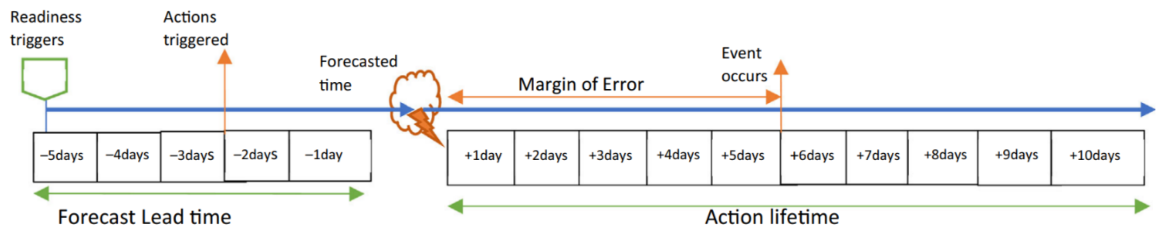

Figure B2: Visual representation of the action lifetime and forecast lead time in a humanitarian aid context, adapted from Mitheu et al. (2023).

Flood event sampling begins by comparing timeseries \$Q(t)\$ against a predetermined threshold \$Q_{th}\$. By doing so, a Boolean mask
\begin{equation}
\text{mask}(t) = \begin{cases}\text{True} & \text{if } Q(t) > Q_{th}, \\
\text{False} & \text{if } Q(t) \leq Q_{th}.
\end{cases}
\end{equation}
is generated for every time step. In case of more than two consecutive *emph{True}*'s, it constitutes a flood; if an exceedance only has a length of one *emph{True},* the river is expected to handle the flood itself. Furthermore, we define the *emph{action lifetime}*: the 10-day period following the initial warning in which action taken remains effective. Any threshold exceedances at the same location within an action lifetime, 10 days before or after, are merged into a single trigger event. This procedure results in events with a location (i.e. a station or district) and a temporal start, end, and duration. The amount of events per data type as a function of threshold is listed in Table~2 in Section~3. We see that, except for the severity-invariant impact data, the amount of events decreases with an increase of threshold. Surprisingly, looking at the observation data sample sizes, the 10-year return period is surpassed a total of 19 times over 13 stations in a period of just 7 years. This can be explained by thresholds being calculated based on a 44-year period of floods starting in 1980, in conjunction with climate change (Hirabayashi et al., 2013).

Where this completes preprocessing for comparison of hindcasts with observational discharges, the impact data analysis requires an extra step because of limited data availability (over the dimensions time and space). To account for missing impact data and to focus on comparative trigger alignment, forecasted events are only included when certain conditions on the presence of impact events are met.

Specifically, forecasted events are excluded when for a particular year no corresponding impact event is found in a particular district. This results in some districts being excluded altogether, and some in select years.

B.4. Evaluating modelled against sampled events

With uniform flood events created for the impact data, observation data, PTM, GloFAS, and GFH forecasts for all lead times and return periods (using impact and observation data), they can now be compared by determining their spatial and temporal overlap. In principle, a binary criterion is adopted: a flood event is considered correctly predicted if it overlaps both spatially (i.e. in the same district or station) and temporally (i.e., for at least one day) with the ground truth (i.e., an impact or observation event). This procedure yields a confusion matrix, Table~B2, for subsequent analysis.

Table B2: Confusion matrix for the predicted events (here called floods).

	Observed flood	No flood observed
Forecast flood	Hit (H)	False Alarm (FA)
No forecast flood	Miss (M)	Correct Negative (CN)

The overlap determination involves several subtleties. Similar to Section~3.32, where the action lifetime was considered when sampling events to emphasise the practical objectives of this research, a similar approach is applied when determining overlap between predictions and observations/impact data. Moreover, it is not uncommon to account for statistical deviations or measurement inaccuracies. Nearing et al. (2024), for instance, considered a forecast correct if the modelled and observed events occurred within two days of each other.

The key skill scores for an EAP trigger development (IFRC, 2025; Sedhain et al., 2025) are the probability of detection (POD)

$$POD = \frac{H}{H + M},$$

and the false alarm ratio (FAR)

$$FAR = \frac{FA}{H + FA}.$$

POD, also known as recall, has a perfect score of 1, while FAR, the complement of precision, has a perfect score of 0. Both range from 0 to 1. A POD > 0.6 and a FAR < 0.3 are generally considered as "Good", and a POD > 0.5 and FAR < 0.5 as "Acceptable" (Duque et al., 2023). We will compare the model scores against these thresholds to get an estimation of their usability.

B.5. Number of events

The workflow resulted in datasets of modelled, observed and impact events, whose sample sizes are listed in Table B3.

Table B3: Total event dataset sizes for Google Flood Hub (GFH), GloFAS v3.0/v4.0, observation hydrographs, and from impact data generated over a period of 7 years. For GFH and GloFAS, it concerns 7-day lead time forecasts (true positives and false positives summed). We see that with an increase of the threshold, n decreases. Note that events generated from hydrographs can represent many underlying datapoints. As a proxy, for observations with a 5-yr RP, mean duration was 22.7 days (SD = 15.9), whereas for the most extreme threshold (10-yr RP), mean duration was 15.4 days (SD = 11.4). GloFAS v3.0 results for percentile thresholds were not calculated. As impact data do not distinguish flood severity levels, impact events are associated to all thresholds/

Analysis	Sample size n						
	95\%	98\%	99\%	1.5-yr	2-yr	5-yr	10-yr
Google Flood Hub	73	62	44	80	78	48	19
GloFAS v3.0	-	-	-	28	21	4	0
GloFAS v4.0	58	55	41	33	23	11	6
Observations	71	61	43	77	73	47	19

Impact data	110	110	110	110	110	110	110

Appendix C. Additional figures

C.1. F1-scores against observation discharges

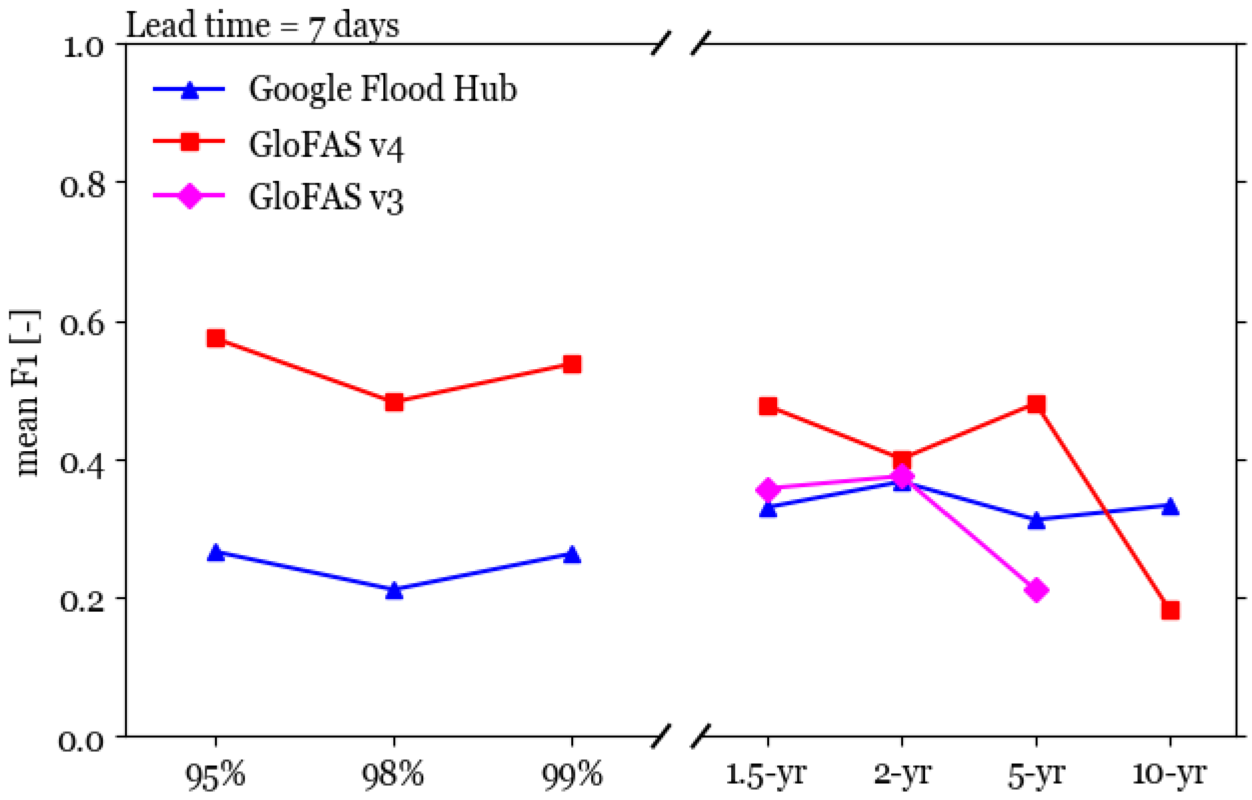

Figure C1: Mean F1-score (harmonic mean of precision and recall) over all stations as a function of threshold (with discharge observations as ground truth) for 7 day lead time. GloFAS v3.0 results for percentile thresholds were not calculated, while for its 10-yr return period, $n = 0$.